Off-fault damage patterns due to supershear ruptures with application to the 2001 M w 8.1 Kokoxili (Kunlun) Tibet earthquake

Harsha S. Bhat, Renata Dmowska, Geoffrey C.P. King, Yann Klinger, James R. Rice

Off-fault damage patterns due to supershear ruptures with application to the 2001 M_w 8.1 Kokoxili (Kunlun) Tibet earthquake

Harsha S. Bhat,[1] Renata Dmowska,[1,2] Geoffrey C. P. King,[3] Yann Klinger,[3] and James R. Rice[1,2]

Received 4 April 2006; revised 11 October 2006; accepted 1 April 2007; published 2 June 2007.

[1] We extend a model of a two-dimensional self-healing slip pulse, propagating dynamically in steady state with slip-weakening failure criterion, to the supershear regime in order to study the off-fault stressing induced by such a slip pulse and investigate features unique to the supershear range. Specifically, we show that there exists a nonattenuating stress field behind the Mach front that radiates high stresses arbitrarily far from the fault (practically this would be limited to distances comparable to the depth of the seismogenic zone), thus being capable of creating fresh damage or inducing Coulomb failure in known structures at large distances away from the main fault. We allow for both strike-slip and dip-slip failure induced by such a slip pulse. We show that off-fault damage is controlled by the speed of the slip-pulse, scaled stress drop, and principal stress orientation of the prestress field. We apply this model to study damage features induced during the 2001 Kokoxili (Kunlun) event in Tibet, for which it has been suggested that much of the rupture was supershear. We argue that an interval of simultaneous induced normal faulting is more likely due to a slip partitioning mechanism suggested previously than to the special features of supershear rupture. However, those features do provide an explanation for otherwise anomalous ground cracking at several kilometers from the main fault. We also make some estimates of fracture energy which, for a given net slip and dynamic stress drop, is lower than for a sub-Rayleigh slip pulse because part of the energy fed by the far-field stress is radiated back along the Mach fronts.

Citation: Bhat, H. S., R. Dmowska, G. C. P. King, Y. Klinger, and J. R. Rice (2007), Off-fault damage patterns due to supershear ruptures with application to the 2001 M_w 8.1 Kokoxili (Kunlun) Tibet earthquake, *J. Geophys. Res.*, *112*, B06301, doi:10.1029/2006JB004425.

1. Introduction

[2] There have been increased recent reports of supershear earthquake ruptures (for which the propagation speed lies between the shear and the dilatational wave speed of the surrounding medium). The earliest inference of supershear was during the 1979 Imperial Valley earthquake for which *Archuleta* [1984] noticed that for a better fit of near-fault strong motion records, the rupture speed had to exceed the shear wave speed. More recent inferences were made during the 1999 Izmit and Düzce events [*Bouchon et al.*, 2000, 2001], the 2001 Kokoxili (Kunlun) event [*Bouchon and Vallee*, 2003], and the 2002 Denali event [*Ellsworth et al.*, 2004]. Laboratory verification of supershear rupture was provided for the first time by *Rosakis et al.* [1999]. However, the theoretical work on these ruptures dates back to the early 1970s when *Burridge* [1973] studied the growth of a self-similar mode-II crack with a critical stress fracture criterion. His work suggested a possible mechanism for the transition of rupture from sub-Rayleigh to supershear regime by formation of daughter cracks ahead of the main crack and their subsequent coalescence. *Andrews* [1976, 1985] subsequently confirmed this in his numerical simulations with a linear slip-weakening failure criterion. *Andrews* [1976] also showed that for a sufficiently low seismic S ratio [$= (\sigma^0_{yx} - \tau_r)/(\tau_p - \sigma^0_{yx})$ where σ^0_{yx}, τ_p, and τ_r are the initial shear stress, peak failure, and residual failure strengths of the medium, respectively], supershear transition of rupture may occur after a propagation distance which scales with the size of the nucleation zone for that σ^0_{yx}. *Burridge et al.* [1979] showed that supershear ruptures whose speed were less than $\sqrt{2}c_s$ (c_s being the shear wave speed of the medium), the Eshelby speed [*Eshelby*, 1949] at which the shear wave contribution (also the Mach front) vanishes, had features suggesting that steady propagation would be unstable, although no complete stability analysis has been done of a steady state rupture. However, the small

[1]Division of Engineering and Applied Sciences, Harvard University, Cambridge, Massachusetts, USA.
[2]Department of Earth and Planetary Sciences, Harvard University, Cambridge, Massachusetts, USA.
[3]Laboratoire Tectonique, Institut de Physique du Globe de Paris, Paris, France.

0148-0227/07/2006JB004425$09.00

set of supershear earthquakes, laboratory, and numerical studies do seem to confirm their analysis. *Bhat et al.* [2004] did find a numerical solution that appears stable at speed $<\sqrt{2}c_s$, but for a supershear rupture emanating from a fault branch that is interacting with a sub-Rayleigh crack from the other arm of the branch.

[3] There remains still, however, much uncertainty about the observation of supershear ruptures in large crustal earthquakes because of the lack of sufficient strong ground motion records. For example, the 2002 Denali event is hypothesized to have propagated at supershear speed for about 40 km [*Ellsworth et al.*, 2004] based on a single ground motion record. Other claims of supershear rupture propagation come mainly from trying to fit a rupture speed for inversion of ground motion data, although, recently, *Dunham and Archuleta* [2005] have identified specific features of the near-fault waveform that indicate supershear rupture and have shown that a record written near the Denali rupture has that form.

[4] The aim of this work is to point out some unique features of supershear ruptures that manifest themselves as patterns of off-fault damage which should be, in favorable circumstances, directly observed in the field. Earlier work by *Poliakov et al.* [2002] and *Rice et al.* [2005] for steady sub-Rayleigh rupture speeds has revealed expected off-fault damage patterns. Those were dependent on rupture speed and orientation of the prestress field among other parameters, and were shown to have some consistency with field observations. We thus adopt the extension by *Dunham and Archuleta* [2005] of the speed regime of Rice et al.'s solution for a steady self-healing slip pulse (right-lateral in nature to be consistent with Poliakov et al., *Kame et al.* [2003], *Bhat et al.* [2004], *Rice et al.* [2005], and *Dunham and Archuleta* [2005]) to the supershear regime, and study the off-fault damage created during rupture propagation. *Dunham and Archuleta* [2005] focused on radiated ground motions.

2. Off-Fault Stress Field due to an Elastodynamic Slip Pulse

[5] Following the work of *Poliakov et al.* [2002], and building on earlier studies of *Broberg* [1978, 1989, 1999], *Freund* [1979], *Rice* [1980], and *Heaton* [1990], *Rice et al.* [2005] calculated the stress field near an elastodynamic slip pulse of length L propagating in steady state at the rupture speed v_r (the speed of the pulse) when v_r was in the sub-Rayleigh wave speed regime (the Rayleigh wave speed is the limiting speed for mode-II ruptures, when the supershear transition can be avoided). They used a nonsingular slip-weakening model [*Ida*, 1972; *Palmer and Rice*, 1973], in a special simplified form introduced by *Palmer and Rice* [1973] in which stress is assumed to vary linearly with spatial position. Weakening begins when shear stress on the fault, τ, first reaches a finite peak strength τ_p on an unslipped part of the fault. When slip begins, τ decreases with slip, approaching τ_r at large slip, as illustrated in Figure 1; the simplified model assumes linear degradation of strength with distance over the slip-weakening zone length R and then a constant strength value over the remaining part of the pulse. The decrease of τ with slip δ is then not linear in δ, but is moderately different from linear, and, in the sub-Rayleigh range, it is independent of v_r for a given R/L and is only weakly dependent on R/L [*Rice et al.*, 2005]. We show later here that a similar feature holds for the supershear range, but with a small dependence on v_r. The peak strength τ_p is generally assumed to be proportional to the compressive normal stress acting on the fault and is set equal to $-f_s(\sigma_{yy})$. We take the static friction coefficient $f_s = 0.6$ based on lab values for typical rocks. The residual strength $\tau_r = -f_d(\sigma_{yy})$ is determined by the dynamic coefficient of friction f_d. We choose $f_d/f_s = \tau_r/\tau_p = 0.2$ as in the works of Poliakov et al. and Rice et al., but note that this number cannot be ascertained precisely. However, some results with appropriately scaled measures of stress changes (scaled with $\sigma^0_{yx} - \tau_r$ or $\tau_p - \tau_r$) do not depend on τ_r/τ_p.

[6] The complete solution for the stress and particle velocity fields associated with the extension of the model to supershear has been derived in the work by *Dunham and Archuleta* [2005].

[7] Let the total stress tensor during the propagation of the slip-pulse be given by $\sigma_{ij} = \sigma^0_{ij} + \Delta\sigma_{ij}$ where σ^0_{ij} and $\Delta\sigma_{ij}$ are the tensors of prestress and perturbation of stress, respectively. The perturbation of the stress field in a homogeneous, isotropic, elastic medium due to a slip pulse propagating at supershear speeds (under plane strain conditions in an unbounded solid) must have a form in terms of a single analytic function $S(z)$ [*Freund*, 1990], such that the stress perturbations are given by

$$\begin{aligned}
\Delta\sigma_{xx} &= \frac{1+\hat{\alpha}_s^2+2\alpha_d^2}{2\alpha_d}\Im S(z_d) + \frac{\hat{\alpha}_s^2-1}{2\alpha_d}\Im S(z_s)\\
\Delta\sigma_{xy} &= \Re S(z_d) + \frac{(\hat{\alpha}_s^2-1)^2}{4\alpha_d\hat{\alpha}_s}\Im S(z_s)\\
\Delta\sigma_{yy} &= \frac{\hat{\alpha}_s^2-1}{2\alpha_d}\Im[S(z_d)-S(z_s)]\\
\Delta\sigma_{zz} &= \nu(\Delta\sigma_{xx}+\Delta\sigma_{yy})
\end{aligned} \tag{1}$$

where $\hat{\alpha}_s = \sqrt{v_r^2/c_s^2 - 1}$; $\alpha_d = \sqrt{1 - v_r^2/c_d^2}$; $z_s = x - v_r t + \hat{\alpha}_s|y|$ and $z_d = x - v_r t + i\alpha_d y$; $i = \sqrt{-1}$; we show results here at time $t = 0$. ν is the Poisson ratio for the medium and is chosen later to be 0.25 so that $c_d = \sqrt{3}c_s$, in our numerical evaluations. c_d and c_s are the P (dilatational) and S (shear) wave speeds of the medium, respectively. $S(z)$, with different arguments, expresses the contributions of the P (dilatational) and the S (shear) waves propagating through the medium; it must be chosen so that the stresses follow the linear strength degradation boundary conditions like in Figure 1. $\Re S(z)$ and $\Im S(z)$ are the real and imaginary parts of $S(z)$, respectively, and following the development of *Dunham and Archuleta* [2005], $S(z)$ is given by

$$S(z) = -\frac{\sin(\pi q)}{\pi} z^{1-q}(z+L)^q \times \int_{-L}^{0} \frac{(\tau(\xi)-\sigma^0_{yx})}{(-\xi)^{1-q}(\xi+L)^q(\xi-z)}\,d\xi \tag{2}$$

Here

$$q(v_r) = \frac{1}{\pi}\tan^{-1}\left[\frac{4\hat{\alpha}_s\alpha_d}{(\hat{\alpha}_s^2-1)^2}\right] \quad (0 \le q \le 1/2) \tag{3}$$

$$\tau(x) = \begin{cases} \tau_r + \left(1+\frac{x}{R}\right)(\tau_p - \tau_r) & \text{for } -R < x < 0 \\ \tau_r & \text{for } -L < x < -R \end{cases} \tag{4}$$

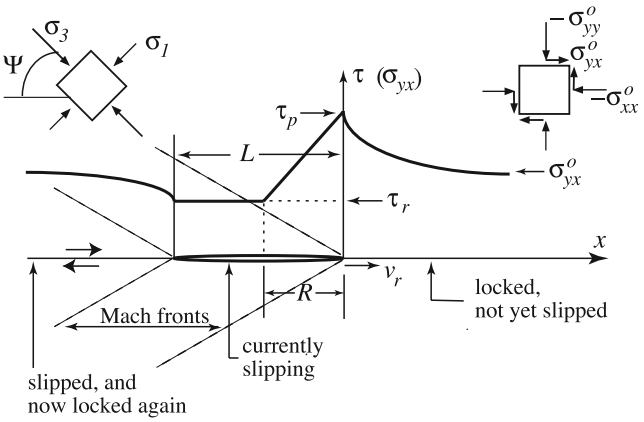

Figure 1. Supershear slip pulse of length L propagating at steady state in a two-dimensional homogeneous elastic medium under plane strain conditions. v_r is the rupture speed limited between the shear wave speed (c_s) and the P wave speed ($c_p = \sqrt{3}c_s$ for Poisson ratio, $\nu = 0.25$) of the medium. The shear strength of the pulse degrades linearly, with distance, from a peak value τ_p to a residual value τ_r over a distance R, the size of the slip-weakening zone. σ^0_{ij} is the prestress in the medium. σ_1 and σ_3 are the minimum and maximum principal compressive stresses, respectively, of the prestress field, in the medium, and Ψ is the angle of inclination of σ_3 with the slip pulse [*Rice et al.*, 2005].

and σ^0_{yx} is the initial shear stress (pre-stress) in the medium. A condition for such a solution to exist, giving bounded stresses at the leading and trailing edges of the pulse, is that $S(z) \to 0$ as $|z| \to \infty$ [*Muskhelishvili*, 1953]. This results in a constraint equation on the shear prestress level which is consistent with a given R/L and v_r. That can be determined as follows. Define

$$\sigma_{\text{drop}} = \frac{\sigma^0_{yx} - \tau_r}{\tau_p - \tau_r} \tag{5}$$

Then

$$\sigma_{\text{drop}} = \frac{I_1}{I_2} \tag{6}$$

where

$$I_1 = \int_0^1 \frac{(1-t)\mathrm{d}t}{(t)^{1-q}(L/R - t)^q};\ I_2 = \int_0^1 \frac{\mathrm{d}t}{(t)^{1-q}(1-t)^q}$$

in nondimensionalized form. Note that since $q = q(v_r)$ is involved, the scaled dynamic stress drop $(\sigma^0_{yx} - \tau_r)/(\tau_p - \tau_r)$ depends on both R/L and v_r/c_s (Figure 2), unlike for its sub-Rayleigh analogue in which case the dependence was only on R/L [*Rice et al.*, 2005]. Similarly $S(z)$ can be nondimensionalized as follows

$$\frac{S(\hat{z})}{\sigma^0_{yx} - \tau_r} = -\frac{\sin(\pi q)}{\pi}\hat{z}^{1-q}\left(\hat{z} + \frac{L}{R}\right)^q \times \left[\frac{R}{L}I_3 - \left(\frac{\tau_p - \tau_r}{\sigma^0_{yx} - \tau_r}\right)I_4\right] \tag{7}$$

where

$$I_3 = \int_0^1 \frac{\mathrm{d}t}{(t)^{1-q}(1-t)^q\left(t + \hat{z}\frac{R}{L}\right)};$$

$$I_4 = \int_0^1 \frac{(1-t)\mathrm{d}t}{(t)^{1-q}\left(\frac{L}{R} - t\right)^q(t + \hat{z})} \text{ and } \hat{z} = \frac{z}{R}$$

3. Nondimensional Parameters in the Model

[8] We now have the perturbation $\Delta\sigma_{ij}$ from the pre-stress field, if normalized by the dynamic stress drop $\sigma^0_{yx} - \tau_r$ or by the strength drop $\tau_p - \tau_r$, expressed in terms of nondimensionalized parameters, namely, z/R, R/L, and v_r/c_s. Refer to section 7 for estimates of the physical size of R. The in-plane prestress is characterized by a nondimensional parameter $\sigma^0_{xx}/\sigma^0_{yy}$ which is a proxy for the angle of inclination of the maximum in-plane principal stress (compressive) with the slip-pulse Ψ measured clockwise from the top of the slip pulse (Figure 1). The in-plane stress components are then given by

$$\begin{aligned}\frac{\sigma^0_{yy}}{\sigma^0_{yx} - \tau_r} &= \frac{-1/f_s}{\sigma_{\text{drop}}(1 - f_d/f_s)} \\ \frac{\sigma^0_{yx}}{\sigma^0_{yx} - \tau_r} &= 1 + \frac{f_d/f_s}{\sigma_{\text{drop}}(1 - f_d/f_s)}\end{aligned} \tag{8}$$

[9] To examine out-of-plane failure modes (reverse or normal faults), we must also assign a value for $\sigma^0_{zz}/\sigma^0_{yy}$. We choose various values for σ^0_{zz} lying between, or equal to one of, the maximum (σ_3) and minimum (σ_1) in-plane compressive principal stresses, determined from the initial in-plane stresses. That is, we consider pre-stress states which are at least as favorable to strike-slip as to normal or to thrust failure (refer to Appendix A1).

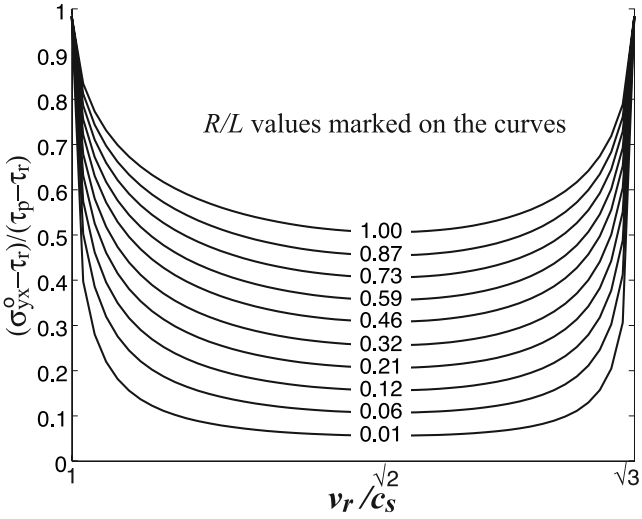

Figure 2. Variation of scaled dynamic stress drop $(\sigma^0_{yx} - \tau_r)/(\tau_p - \tau_r)$ with rupture speed v_r and R/L where R and L are the size of the slip-weakening zone and the length of the slip pulse, respectively. τ_p and τ_r are the peak and residual strengths, respectively, and σ^0_{yx} is the initial shear stress.

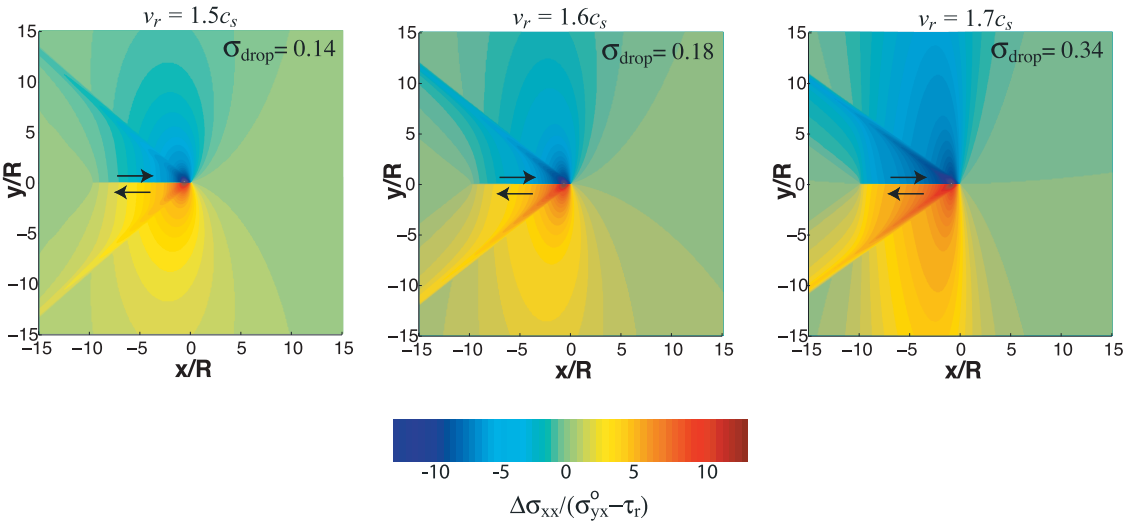

Figure 3. Perturbation in fault parallel stress, $\Delta\sigma_{xx}/(\sigma^0_{yx} - \tau_r)$ normalized by dynamic stress drop because of a supershear slip pulse propagating steadily at various rupture speeds v_r. All results are for $R/L = 0.1$ where R and L are the size of the slip-weakening zone and the length of the slip pulse, respectively, and $\sigma_{drop} = (\sigma^0_{yx} - \tau_r)/(\tau_p - \tau_r)$.

[10] Thus the model has six nondimensional parameters that need to be declared a priori (if the total stress tensor is to be evaluated), namely, v_r/c_s, R/L, f_s, f_d/f_s, $\sigma^0_{xx}/\sigma^0_{yy}$, and $\sigma^0_{zz}/\sigma^0_{yy}$. On this list, σ_{drop} can replace R/L (Figure 2).

4. Off-Fault Stressing due to a Supershear Slip Pulse

[11] Supershear ruptures differ from their sub-Rayleigh analogues in many different ways. The stressing due to the *P* and the *S* waves in the medium is almost decoupled. The *S* wavefield stresses the region only behind the Mach front emanating from the rupture front. In case of a slip pulse, as studied here, two Mach fronts develop at the leading and the trailing edge of the slip pulse, and the band between these fronts defines the *S* wave stressing region (Figure 1). Within the band, the stress field is nonattenuating with distance and is constant (neglecting the modest, attenuating, contributions of the *P* wavefield) along lines parallel to the leading Mach front. The nonattenuation feature in the band is a unique signature of supershear pulses which could potentially lead to damage at distances far away from the slip pulse. The three-dimensional nature of the actual problem presumably restricts this distance to be of the order of the depth of the seismogenic zone (once the rupture saturates in depth, the dominant length scale in the problem is related to this depth and three-dimensional effects can no longer be ignored), usually around 10–15 km. However, this distance is still substantial and of the order of a few tens of kilometers.

[12] Outside the Mach band, the stressing is only due to the *P* waves and attenuates with distance. However, as the rupture speed approaches the upper limiting speed, i.e., the *P* wave speed of the surrounding medium, the Lorentz-like contraction of the stressing region in the fault parallel direction (with a corresponding extension in the fault normal direction) also increases significantly leading to a greater extent of the *P* wave stressing region in the medium hosting the slip pulse. Once again, we notice a greater spatial influence by supershear ruptures compared to sub-Rayleigh ruptures. Figure 3 showing the perturbation in $\Delta\sigma_{xx}$ illustrates the nonattenuating and Lorentz-like contraction features of supershear ruptures.

[13] To characterize the off-fault stressing induced by a supershear slip pulse, we look at the change of Coulomb stress (CS) on fault structures with assumed orientations, and also on structures which are optimally oriented for Coulomb failure based on the total stress tensor. Note that in calculating dynamic Coulomb stress changes on optimally oriented structures and in the evaluation of off-fault failure, all the six nondimensional parameters are to be specified. However, when evaluating the change in the dynamic Coulomb stress on fault structures with assumed orientations, only three nondimensional parameters need to be specified (if stresses are normalized by the dynamic stress drop) a priori, namely, v_r/c_s, R/L, and f_s.

[14] We evaluate the change in the Coulomb stress $\Delta CS = \Delta\tau + f_s\Delta\sigma$ (here $\Delta\tau > 0$ in the direction of possible slip and $\Delta\sigma > 0$ for tension) on faults, both optimally oriented and the ones with assumed orientations, at each grid point, and only the region where failure is encouraged is contoured, i.e., the region where $\Delta CS > 0$. The optimal orientation was determined from the final stress state. We also evaluate Coulomb stress changes for structures slipping out of the plane, i.e., normal and reverse faults. Refer to Appendix A for more details.

5. The 2001 M_w 8.1 Kokoxili (Kunlun) Earthquake

[15] The Kokoxili surface rupture (Figure 4) has been studied by a number of workers (*Xu et al.* [2002], *Lin et al.* [2002, 2003], *Lasserre et al.* [2005], and *Klinger et al.* [2006], among others) and mapped in detail using Ikonos satellite images and supporting fieldwork by *Klinger et al.* [2005]. Particular attention was paid to the slip-partitioned section, which is also discussed by *King et al.* [2005].

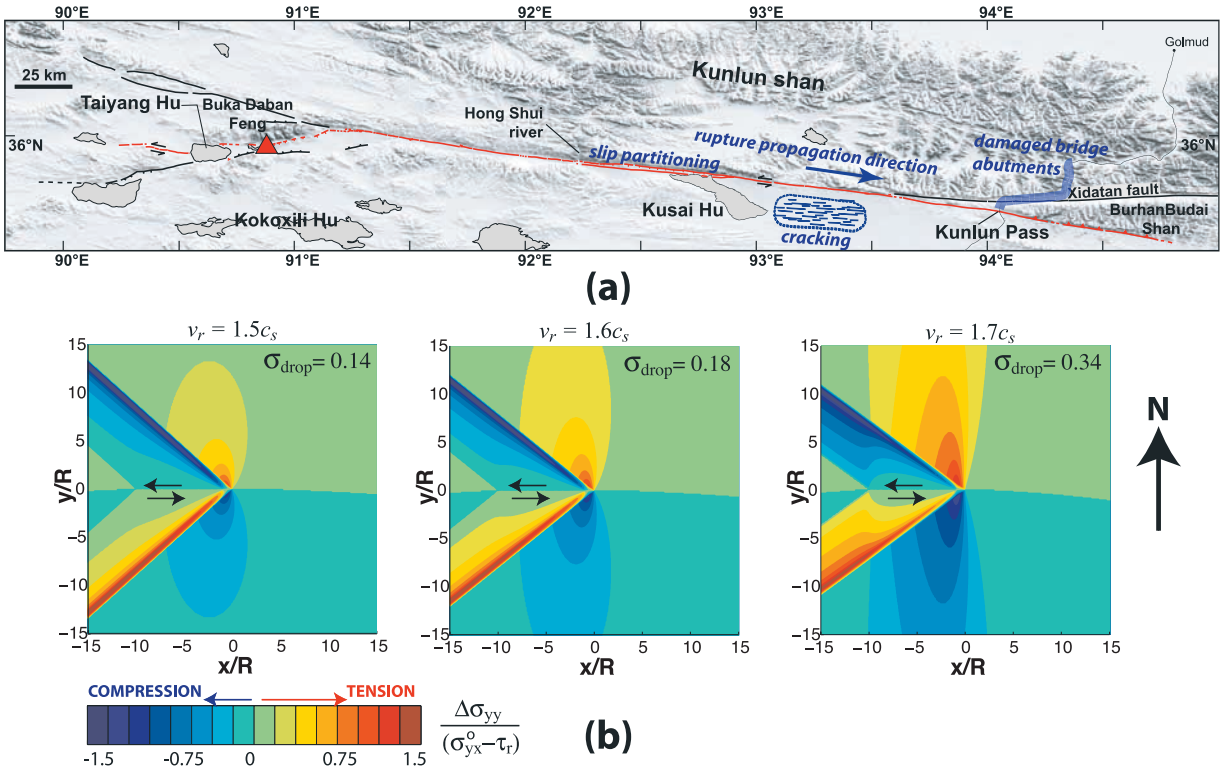

Figure 4. (a) Simplified map of the surface rupture (red line) for the 2002 Kokoxili earthquake (adapted from *Klinger et al.* [2005]). Epicenter is indicated by a red triangle so that rupture propagated mainly to the east. The slip-partitioned section extends from the Hong Shui river to north of the middle of Kusai Hu (lake). Extensive cracking was observed (with approximate crack orientations drawn by authors) from east of the Kusai Hu to about halfway to the Kunlun Pass. North of the pass (where the road to Golmud is outlined in blue) bridge abutments were damaged. The extent of the region of cracking parallel to the strike of the fault is likely to be correct, but the extent perpendicular to it is simply not determined, and it is only sure that the cracking extended to the horizon on both sides of the road. (b) Perturbation in fault normal stress $\Delta\sigma_{yy}/(\sigma^0_{yx} - \tau_r)$ normalized by dynamic stress drop because of a "left-lateral" supershear slip pulse propagating steadily at various rupture speeds v_r (all other figures in this paper are drawn for right-lateral slip). The results are for $R/L = 0.1$ where R and L are the size of the slip-weakening zone and the length of the slip pulse, respectively, and $\sigma_{drop} = (\sigma^0_{yx} - \tau_r)/(\tau_p - \tau_r)$.

Kikuchi and Yamanaka [2001], *Lin et al.* [2003], *Bouchon and Vallee* [2003], *Antolik et al.* [2004], *Tocheport et al.* [2006], and *Robinson et al.* [2006] did seismological studies of the rupture process associated with the Kokoxili event. The field team noted other interesting features, but unfortunately could not study them in detail so that we do not have careful field documentation. Thus although the observations may be consistent with rupture propagation at supershear speeds, the correlation should be treated with caution.

[16] North of the fault, bridge abutments crossing minor drainages on the Kunlun Pass to Golmud road were damaged. Since fragile walls and poorly constructed buildings were undamaged even closer to the fault and such bridges are not normally sensitive to shaking, a likely explanation is that the damage resulted from large ground strains probably in extension. The damage did not appear to be due to compression, although, without more careful examination, it cannot be excluded.

[17] South of the fault, on the road between the Kunlun Pass and Kusai Hu, extensive ground cracking occurred (Figure 5) oriented at approximately fault parallel as shown in Figure 4a. The cracking was not mapped since the cracks were too small to appear on Ikonos images. Direct mapping of a large region would have required an extended period at an altitude of nearly 4000 m which was not possible. The extent of the region of cracking (shown in Figure 4) parallel to the strike of the fault is likely to be correct, but the extent perpendicular to it is simply not determined, and it is only sure that the cracking extended to the horizon on both sides of the road. Whether or not the map is accurate, the cracks were substantial distributed features that did not have the character of primary fault ruptures. The field team did not constrain the orientation of these features relative to the main Kokoxili rupture trace. However, the road track shown in Figure 5 is roughly oriented in the west-north-west direction (the absence of the Kunlunshan mountain range at the horizon of Figure 5 supports this conclusion). That means that the cracks are oriented at shallow angles to the main rupture trace. Our estimates of the far-field stresses (Appendix B) show that, for a left-lateral supershear rupture as the Kokoxili event, the region where the cracks were observed suffered from large fault normal extensional stress perturbation ($\Delta\sigma_{yy} \approx 5$–$15$ MPa for a 3-MPa dynamic stress drop,

Figure 5. Cracks along the road from Kusai Hai to the Kunlun pass. At this point, the road is several kilometers from the fault. The cracks were not mapped and their orientation was not specifically measured, but was close to the orientation shown in Figure 4. The cracking is consistent either with extension or with compression and inelastic yielding followed by tensional failure when the compression was relaxed.

on the pulse, consistent with the average stress drop inferred by *Rice et al.* [2005] for other large, sub-Rayleigh ruptures) leading to the formation of tensile cracks oriented roughly parallel to the main rupture trace [Figure 4b].

[18] Because there is only the limited constraint mentioned of the cracking direction, it is instructive to examine other possibilities. If these extensional features were oriented at some near-perpendicular angle to the main rupture trace, then this could mean that the extensional features observed were created by the unloading phase following the traversal of a large compressional loading pulse. For such orientation, it would be possible that the brittle near-surface material (frozen soil sediments) could yield in compaction when the Mach front traversed through the material, and then unloaded as tensile cracks when the compressional strain was removed in the wake of the Mach front. Our estimates of far-field stresses (see Appendix B) show that at Kunlun rupture speeds, the fault parallel stress perturbation ($\Delta\sigma_{xx}$) is compressional and quite large ($\approx$5–15 MPa) for a 3-MPa dynamic stress drop on the pulse [Figures 3 and 6]. Thus there is a plausible mechanism for any angle of the tensile cracks with respect to the main fault trace, except for angles in the vicinity of ±45°, in which case the normal stress on these features (whether tensile or compressive) is small in magnitude.

[19] We also checked for the possibility of normal and thrust structures, striking perpendicular to the slip pulse, being activated because of the supershear slip pulse. Figure 7 shows the change in the dynamic Coulomb stress on such structures. Note that the southern side of Kunlun (left lateral) is the $y > 0$ domain in our model (right lateral). (Also, in the interpretation for left-lateral faulting, in our figures, we are not looking down onto Earth's surface from space, but rather up to the

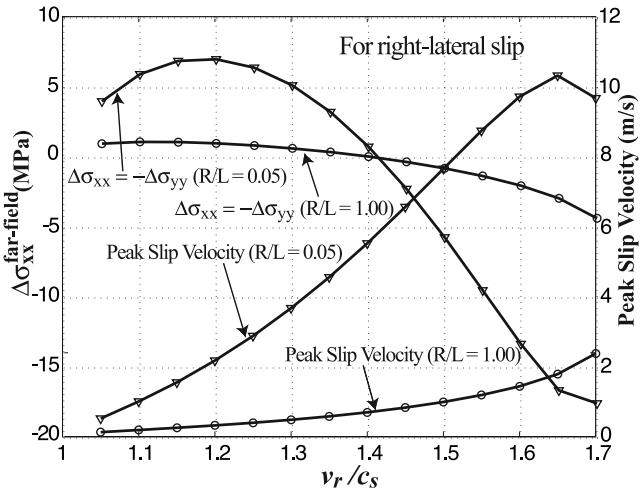

Figure 6. Far-field perturbation in fault parallel stress $\Delta\sigma_{xx}$ as a function of rupture velocity calculated using the maximum slip velocities at the corresponding rupture velocities and for different values of R/L. We assume dynamic stress drop to be 3 MPa, shear modulus to be 30 GPa, and S-wave speed of 3 km/s in these calculations.

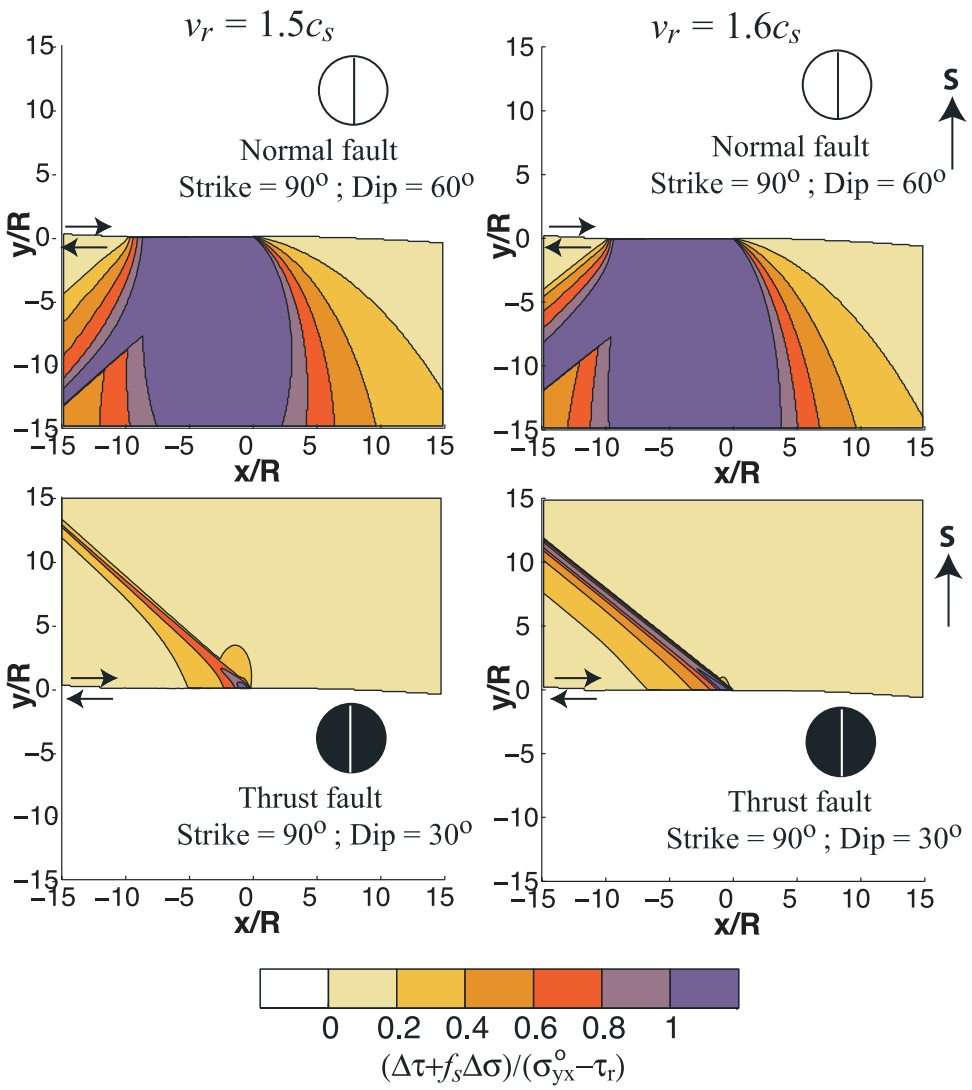

Figure 7. Contours of positive change in Coulomb stress (scaled by dynamic stress drop), due to a supershear rupture, on normal and thrust faults striking perpendicular to the slip pulse and dipping at 60° and 30°, respectively. Open circle represents normal faults and shaded circle represents thrust faults with their strike shown by the bisecting line.

surface from the interior.) The figure clearly shows that thrust faulting structures (striking perpendicular to the slip pulse) could be activated in the southern side of Kunlun at large distances. In fact, the region of highest positive change in the dynamic Coulomb stress lies along the leading Mach front which extends to distances comparable to the seismogenic depths in our two-dimensional model.

[20] At sub-Rayleigh speeds ($0.7-0.9c_s$) at a distance of 5 km (using *Rice et al.*'s [2005] estimates of R_0^* (size of the slip-weakening zone for a static semi-infinite crack), an average value of 30 m used here, and factoring in the Lorentz-like contraction of R, this would correspond to approximately $250-1000R$), the stresses are quite negligible, at around 0.1% of dynamic stress drop. Thus a sub-Rayleigh rupture could not have created features discussed above.

[21] *Klinger et al.* [2005] have mapped in detail that a normal fault strand, about 70 km long, striking parallel to the Kunlun fault at a distance of approximately 1–2.5 km to the north of Kunlun slipped during the 2001 event (see the slip-partitioned section in Figure 4). The rupture speed is constrained by the inversion studies of *Bouchon and Vallee* [2003] to be between 1.5 and $1.6c_s$. *King et al.* [2005] have related the activation of this normal strand during the event to slip partitioning at depth where the normal and strike-slip structures are connected. We look for direct Coulomb stress changes on the normal fault strand due to a supershear rupture on an adjacent fault to see if supershear ruptures could activate such features and possibly provide a complementary mechanism. Figure 8 shows this change in Coulomb stress for normal faulting structures striking parallel to the main slip pulse and dipping at 60°. Since Kunlun is a left-laterally slipping fault and our calculations are for a slip pulse slipping right laterally, the northern side of Kunlun represents $y < 0$ domain in our figure (looking toward the Earth's surface from beneath). Normal faulting, in the $y < 0$ domain, is discouraged (negative change in Coulomb stress) in the nonattenuating part of the field when

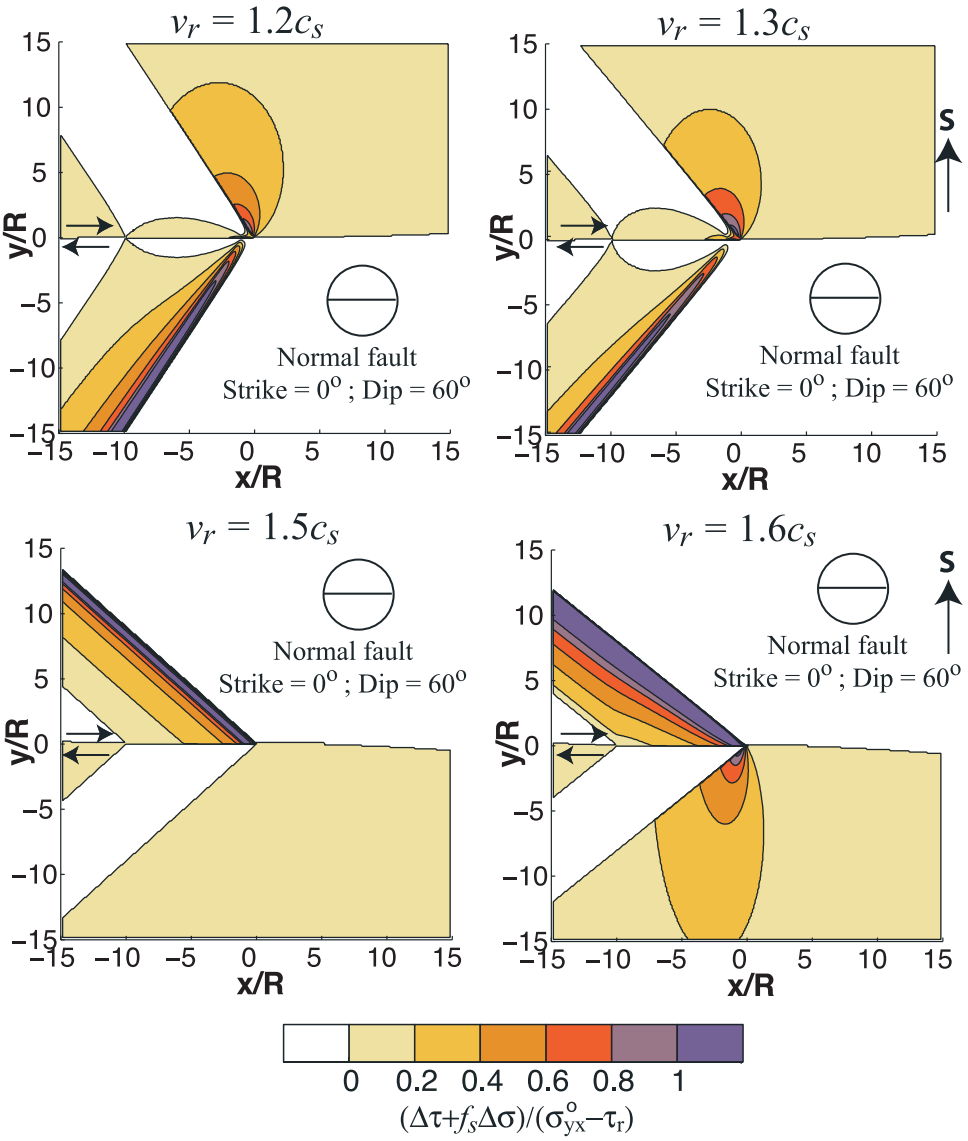

Figure 8. Contours of positive change in Coulomb stress (scaled by dynamic stress drop), due to a supershear rupture, on normal faults striking parallel to the slip pulse and dipping at 60°. Open circle represents normal faults with their strike shown by the bisecting line.

a supershear slip pulse propagates on the main fault at speeds like those inferred, $v_r > \sqrt{2}c_s$.

[22] Though normal faulting is favored in the attenuating part of the stress field (corresponding to the *P* wavefield) at higher speeds, the extent of this field, corresponding to 20% of dynamic stress drop, is only up to 200–300 m (taking $R_0^* = 30$ m and referring to Figure 15). There is a positive change at speeds $v_r < \sqrt{2}c_s$, but these speeds, especially in the range $1.2-1.3c_s$ at which the effects become numerically significant, are thought unlikely.

[23] Since Coulomb stress changes are significant at short distances for all rupture velocities considered here, a supershear slip pulse might have nucleated the normal faulting event at, or near, its junction with the strike-slip strand.

[24] We note that the above-mentioned mechanism of nucleating normal faulting event is, however, not unique to the supershear regime as discussed below. Similar calculation in the sub-Rayleigh speed regime shows that the positive change in the Coulomb stress is quite low (around 1% of the dynamic stress drop) at a distance of about $20R$ from the main fault. Using the data of *Rice et al.* [2005] on R_0^* and factoring in the Lorentz-like contraction of R, the above distance would be roughly between 100 and 400 m.

[25] Thus it seems most unlikely that a sub-Rayleigh rupture could have activated the normal fault structure. We thus find that at the rupture speeds for the Kunlun event, normal fault activation by positive changes in Coulomb stress on the same is unlikely to happen, and no viable alternative is provided to the hypothesis that the normal faulting resulted from slip partitioning at depth [*King et al.*, 2005].

[26] The value of Ψ [defined earlier (Figure 1) and bearing in mind that the fault is left-lateral] about 200 km to the east of the Kunlun-Xidatan junction was estimated to be between 30° and 45° from orientations of active faults in the region. It was noted for Denali fault in Alaska, which

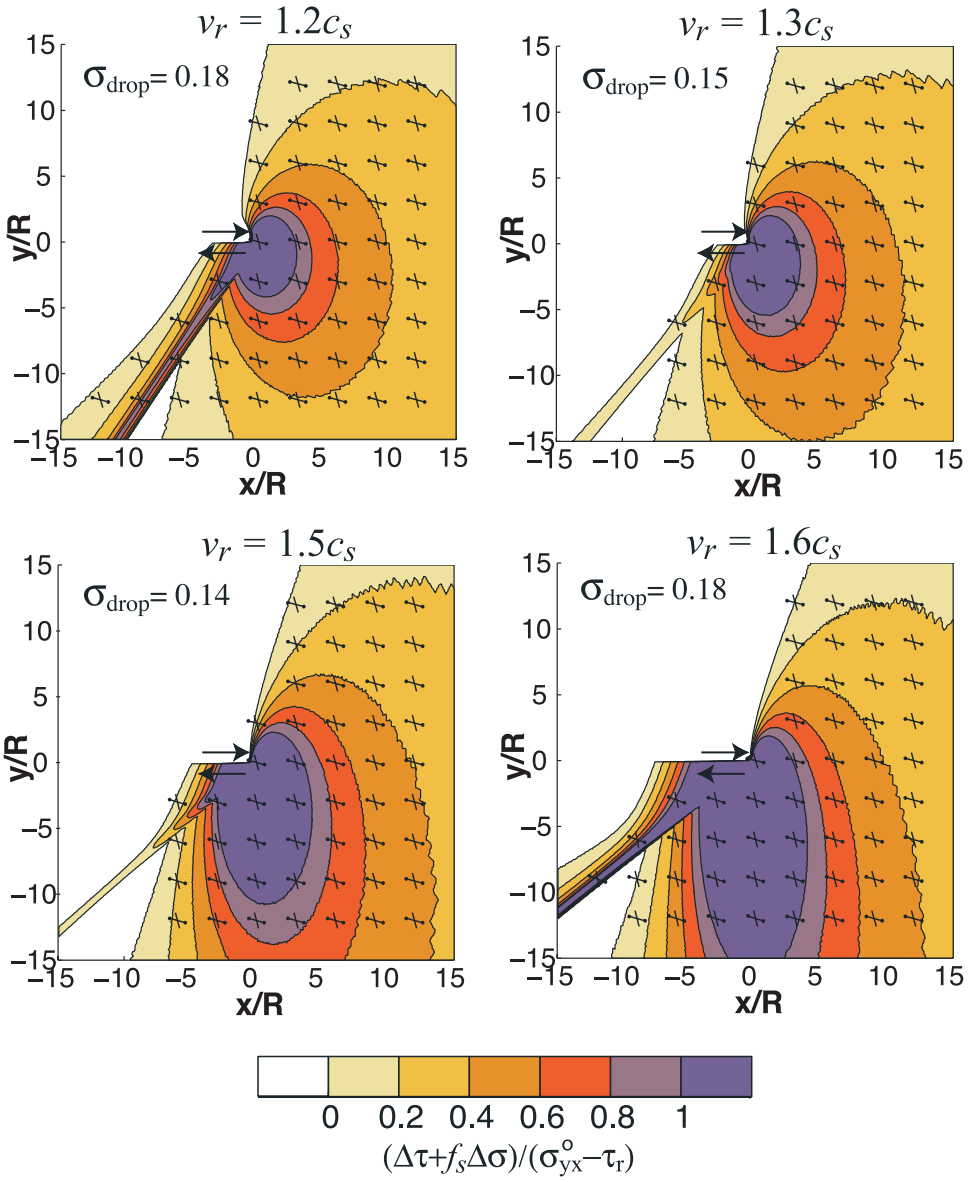

Figure 9. Effect of rupture velocity on positive Coulomb stress changes (maximum of the two on optimally oriented structures) induced by an intersonic slip pulse on optimally oriented structures. Here $\Psi = 45°$ and $\sigma_{drop} = (\sigma^0_{yx} - \tau_r)/(\tau_p - \tau_r)$. σ^0_{zz} is chosen such that the prestress field favors pure strike-slip faulting. Dumbbell-shaped lines represent optimal right-lateral strike-slip structures, and simple lines represent left-lateral strike-slip structures.

has similar tectonic features as Kunlun, by *Ratchkovski* [2003] that the orientation of the maximum principal stress rotated about the normal to the strike as one traversed along the strike of the fault. This might be the case with Kokoxili, but no similar stress direction estimate exists for the region to the east as of now. The orientation of the cracks and the existence of both normal and strike-slip structures gives us an additional constraint on Ψ. First, if the cracks were created by the unloading phase following the traversal of a large compressional loading pulse, then the orientation of the cracks might give us some constraint on the direction of the maximum in-plane compressive stress Ψ. The average orientation of the cracks seem to be between 50° and 55° (no precise measurements were made in the field) with respect to the fault, and these features are expected to form perpendicular to the maximum in-plane compressive stress direction, provided that the stress perturbation added to that compression. This suggests that Ψ should be roughly between 35° and 40°. The simultaneous existence of normal and strike-slip faulting, if interpreted (too strictly) to mean that the τ/σ were the same on both the structures, that σ_{zz}, the maximum principal compressive stress, and the remaining principal stresses be compressive and not greater than σ_{zz}, puts Ψ in the range of 16° to 27° (for τ/σ between 0.3 and 0.6). The direction $\Psi_{\Delta\sigma}$ of the principal compression in the perturbation far field lies between 0° and 10° when $v_r > \sqrt{2}c_s$, specifically between 3° and 6° when $1.5c_s < v_r < 1.6\ c_s$. In fact, in the far field, $\Psi_{\Delta\sigma} = 0.5 \tan^{-1}(-\cot 2\beta)$ where $\sin\beta = c_s/v_r$. For the far-field compressive stress along the principal direction to become yet more compressive, we must have Ψ

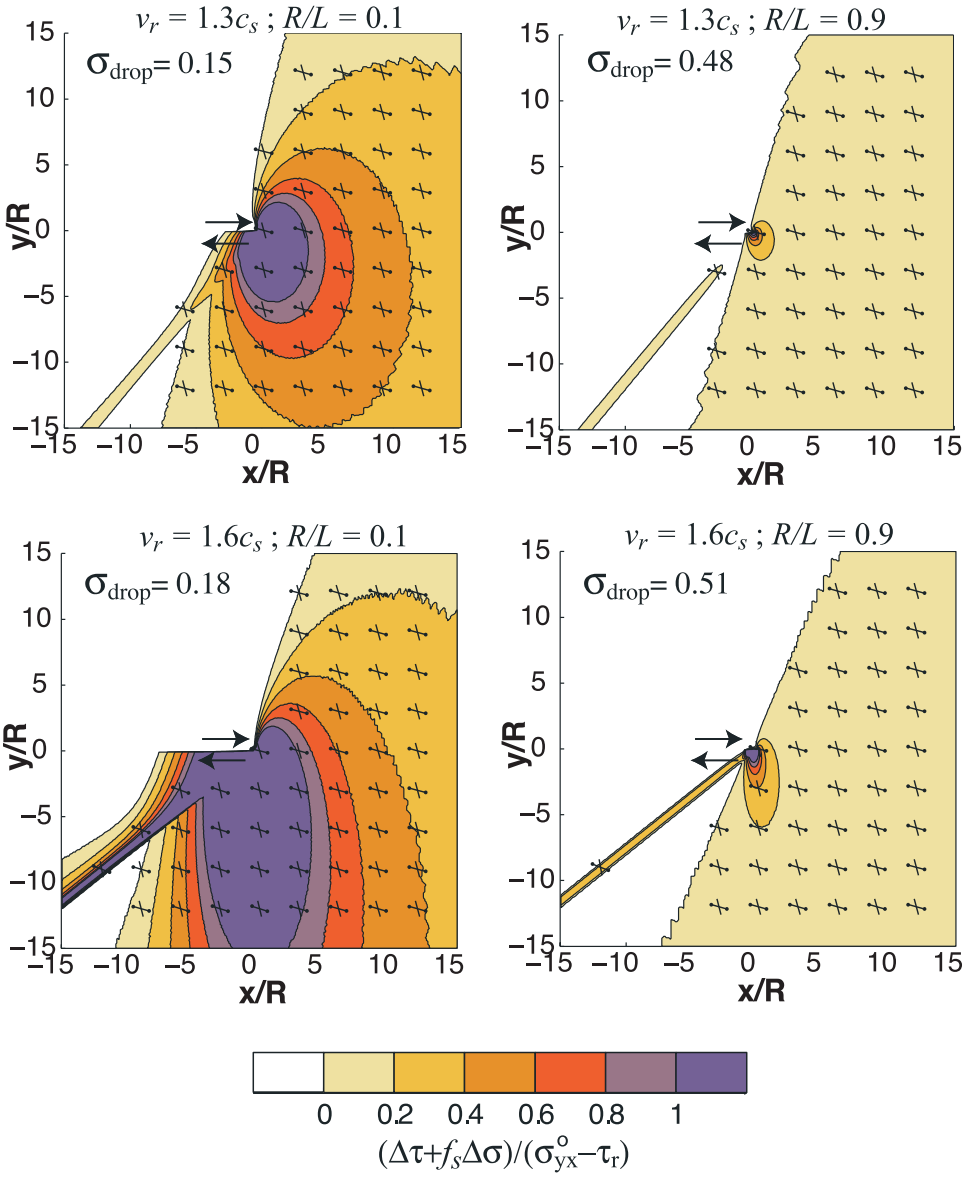

Figure 10. Effect of the size of the slip-weakening zone relative (R) to the length of the slip pulse (L) on Coulomb stress changes (maximum of the two on optimally oriented structures) induced by an intersonic slip pulse on optimally oriented structures. Here $\Psi = 45°$. σ^0_{zz} is chosen such that the prestress field favors pure strike-slip faulting. Refer to Figure 7 for explanation of symbols.

$-\Psi_{\Delta\sigma} < \pi/4$ which implies that $\Psi < \pi/4 - 0.5\tan^{-1}(\cot 2\beta) = 39°$ to $42°$ when $1.5c_s < v_r < 1.6\,c_s$. Thus the above constraints on prestress direction make it plausible that stresses in the far field caused the ground cracking.

6. Effect of Various Model Parameters on the Change in Dynamic Coulomb Stress

[27] Since the perturbation in the elastic field due to S-wave radiation from a supershear slip pulse extends to infinity in our two-dimensional model (practically this would be limited to the depth of the seismogenic zone), we expect significant effects at larger distances from the supershear slip pulse than its sub-Rayleigh analogue. Below we will explore the influence of various nondimensional model parameters, outlined earlier, on off-fault damage. This is done generically without specific application to the Kokoxili event. All the figures have the maximum positive change in Coulomb stress, due to a supershear pulse, contoured for an optimally oriented structure at each grid point.

6.1. Effects of v_r and R/L

[28] The effects of rupture velocity and R/L on the off-fault stress field (for optimally oriented structures) are shown in Figures 9 and 10. These results were obtained for $\sigma^0_{xx}/\sigma^0_{yy} = 1.0$ ($\Psi = 45^0$), $R/L = 0.1$, and σ^0_{zz} chosen such that prestress favors strike-slip faulting, i.e., $\sigma^0_{zz} = 0.5$ ($\sigma_1 + \sigma_3$). With increasing rupture velocity and decreasing R/L, the off-fault stressing, in a medium hosting a supershear slip pulse, increases. Both cases show significant far-field effects on the extensional side of the fault and increasing near field effects (outside the Mach front) with

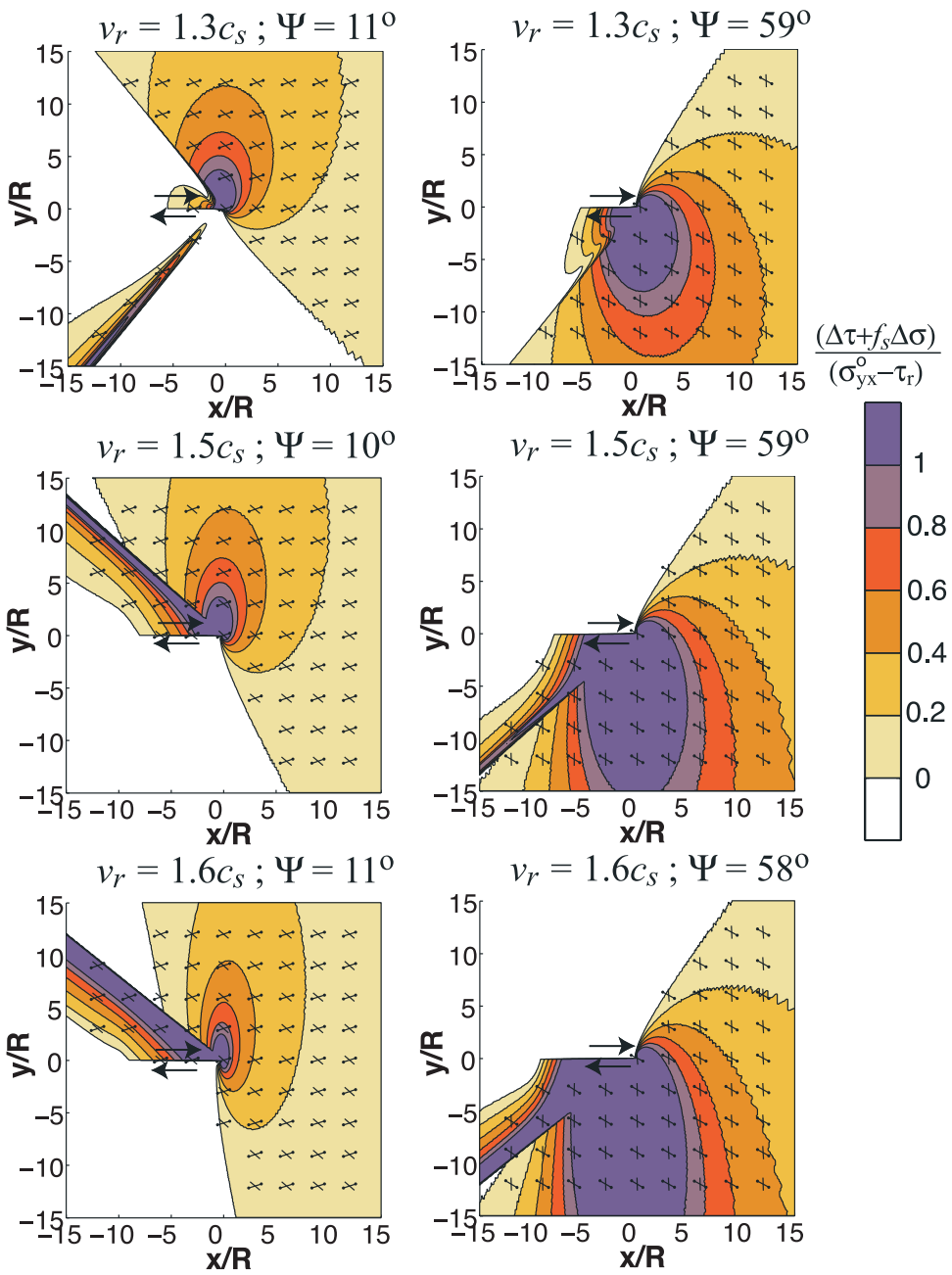

Figure 11. Effect of Ψ on positive Coulomb stress changes (maximum of the two on optimally oriented structures) induced by an intersonic slip pulse on optimally oriented structures. σ^0_{zz} is chosen such that the prestress field favors pure strike-slip faulting. Refer to Figures 6 and 7 for explanation of symbols.

increasing rupture velocity. Increasing R/L results in a reduction in the stress concentration ahead of the rupture tip resulting in reduced off-fault stressing.

6.2. Effect of Ψ

6.2.1. Prestress Favors Pure Strike-Slip Faulting [$\sigma^0_{zz} = 0.5(\sigma_1 + \sigma_3)$]

[29] We consider two different $\sigma^0_{xx}/\sigma^0_{yy}$ ratios, 2.0 and 0.8, for which $\Psi = 10°-11°$ and $58°-59°$, respectively. The slight variation in Ψ is due to the fact that σ^0_{xy} varies with rupture velocity. We consider the effects of the above parameters for $v_r = 1.3$, 1.5, and $1.6c_s$. As seen in Figure 11, switching from low value of Ψ to a higher value results in the shift of the domain of positive Coulomb stress change from mainly on the compressional side to mainly on the extensional side.

6.2.2. Prestress Equally Favors Both Thrust and Strike-Slip Faulting ($\sigma^0_{zz} = \sigma_1$)

[30] As in the previous subsection, the region where there is a positive change in Coulomb stress switches from being predominantly on the compressional side to the extensional side as Ψ is increased. The region of maximum increase Coulomb stress change also increases with rupture velocity (Figure 12).

6.2.3. Prestress Equally Favors Both Normal and Strike-Slip Faulting ($\sigma^0_{zz} = \sigma_3$)

[31] Referring to Figure 13, we see that the same general features outlined earlier stand out. The main difference

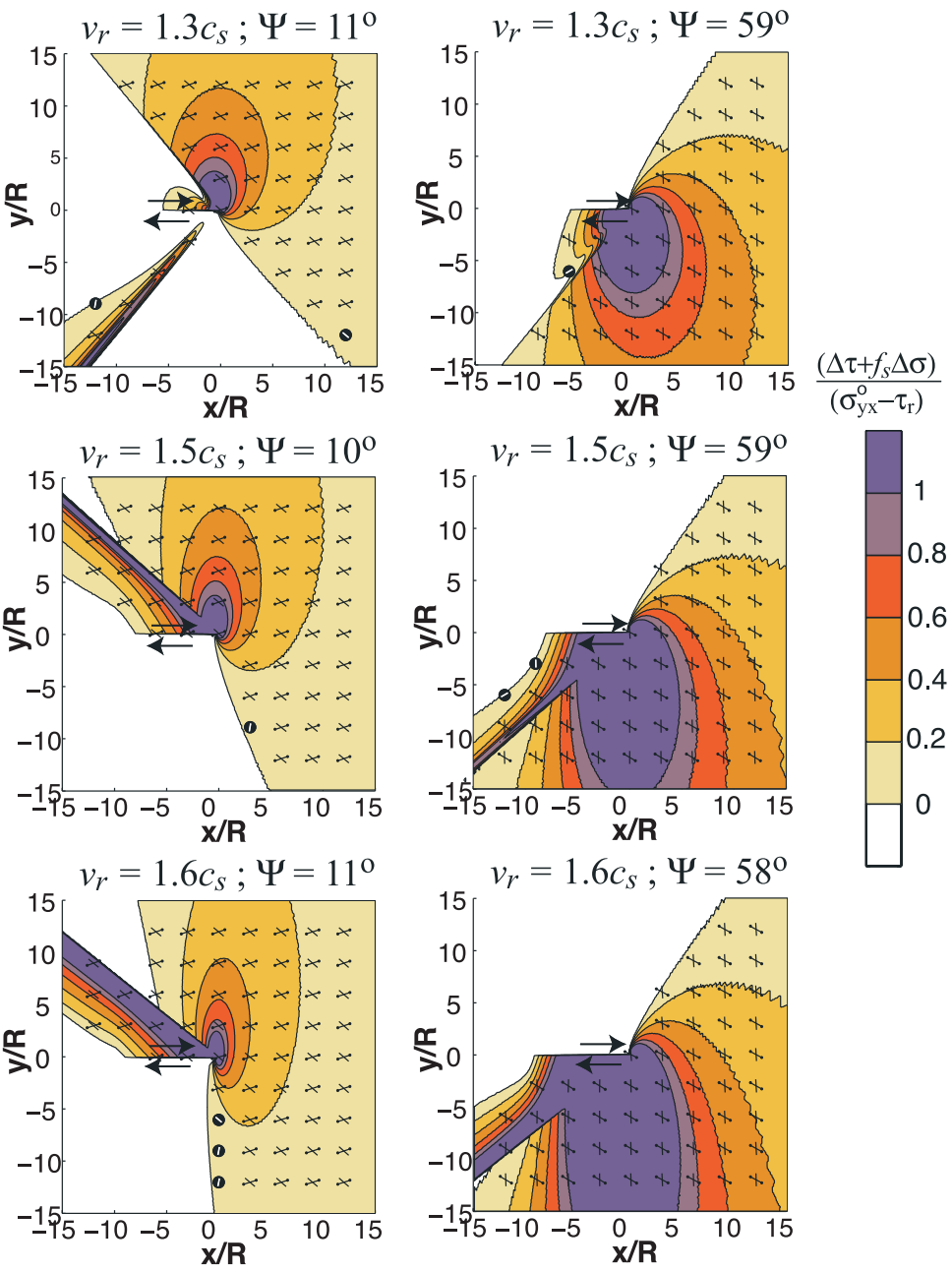

Figure 12. Same as Figure 11 except σ^0_{zz} is chosen such that the prestress field favors equally both strike-slip and thrust faulting. Refer to Figures 6 and 7 for explanation of symbols.

between the three cases discussed is the nature of faulting which follows again the choice of prestress parameters.

7. Energy Balance and Estimates

[32] As explained in the work of *Dunham and Archuleta* [2005], the proper energy balance for a supershear slip pulse is given by $\sigma^0_{yx}\delta = \tau_r\delta + G_{\text{frac}} + G_{\text{rad}}$, where σ^0_{yx} is the far-field shear stress, τ_r is the residual strength of the fault, and δ is the locked-in slip left in the wake of the slip pulse. Here $\tau_r\delta$ is the dissipation at the residual strength level, G_{frac} is the dissipation at stresses excess of the residual which defines the fracture energy, and G_{rad} is the energy flow away from the slip pulse associated with the S waves.

[33] The locked-in slip δ is given by the expression,

$$\frac{\delta}{R} = \frac{1}{v_r}\int_0^{L/R} V(\xi)\mathrm{d}\xi \tag{9}$$

where V is the slip velocity distribution which depends on R/L and v_r/c_s and is given by $V(\xi) = -2v_r[(\alpha circ;_s^2 + 1)/4\mu\alpha_d]\Im S(\xi)$ when approaching the fault from $y > 0$ and ξ denotes x/R. G_{frac} is given by

$$\frac{\mu G_{\text{frac}}}{(\tau_p - \tau_r)^2 R} = \int_0^1 V^*(\xi)(1-\xi)\mathrm{d}\xi \tag{10}$$

where $V^*(\xi) = \mu V(\xi)/[(\tau_p - \tau_r)v_r] = -2\{(\alpha circ;_s^2 + 1)/[4\alpha_d(\tau_p - \tau_r)]\}\Im S(\xi)$. G_{rad} is then evaluated from the

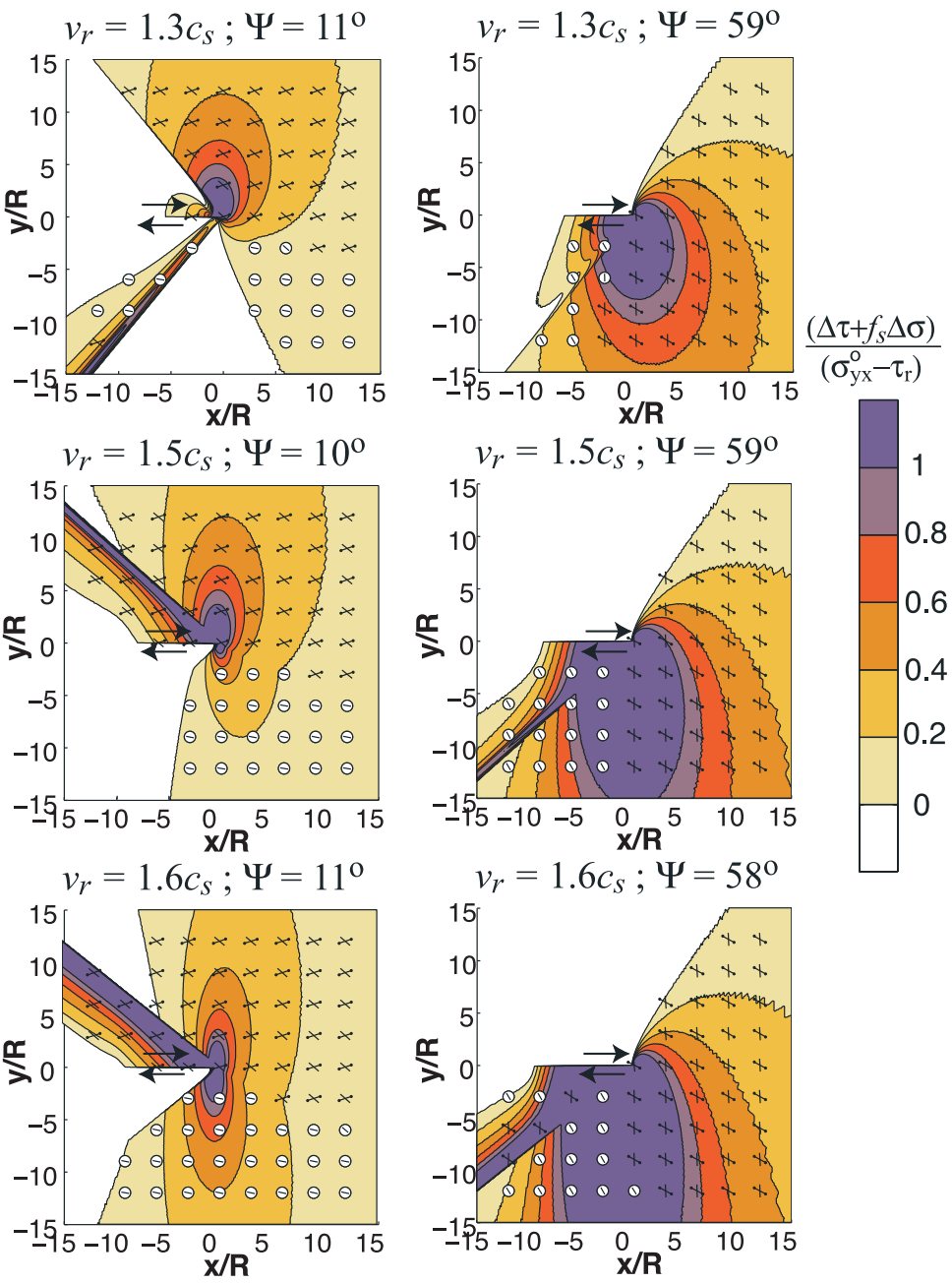

Figure 13. Same as Figure 11 except σ^0_{zz} is chosen such that the prestress field favors equally both strike-slip and normal faulting. Refer to Figures 6 and 7 for explanation of symbols.

energy balance equation. The energy flux associated with G_{rad} extends all the way to infinity and vanishes when the rupture velocity is $\sqrt{2}c_s$. We nondimensionalize energy in our model, following *Rice et al.* [2005], with seismically observable parameters, as $\hat{G} = \pi LG/\mu\delta^2 = F(v_r/c_s, R/L)$ where μ is the shear modulus of the medium hosting the slip pulse. The nondimensional function F cannot be reduced to a simple analytical expression, as in the sub-Rayleigh case, but has to be numerically determined. Also, unlike the sub-Rayleigh case, the dependence of F on rupture speed and R/L is no longer separable. Figure 14 shows the variation of G_{frac} and G_{rad} with rupture velocity for a fixed ratio of dynamic stress drop to strength drop, $(\sigma^0_{yx} - \tau_r)/(\tau_p - \tau_r) = 0.3$. The total energy $G_{frac} + G_{rad}$ decreases monotonically with increasing fracture energy. Since this ratio is dependent on both the rupture speed and the size of the process zone with respect to the length of the slip pulse, we have to vary R/L with rupture velocity to obtain the energy values at fixed stress drop.

[34] One can also use the energy balance equation to evaluate how the size of the slip-weakening zone R varies with R/L and v_r/c_s. We scale this value of R with the size of the process zone at static limit for a semi-infinite crack R_0^* as in the work of *Rice et al.* [2005] where

$$R_0^* = \frac{9\pi}{16(1-\nu)} \frac{\mu G_{frac}}{(\tau_p - \tau_r)^2} \tag{11}$$

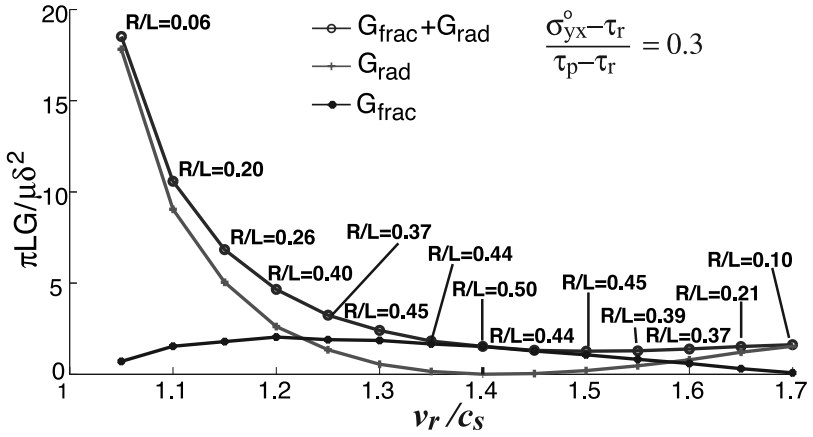

Figure 14. Scaled fracture energy release rate (G_{frac}), energy radiated by S wave (G_{rad}), and the total energy as a function of rupture speed (v_r) for $(\sigma^0_{yx} - \tau_r)/(\tau_p - \tau_r) = 0.3$.

Here v is the Poisson ratio of the medium, set at 0.25 in our model, and G_{frac} is the fracture energy release rate. Using this with equation (11), we get R/R_0^*.

[35] Figure 15 shows the variation of R/R_0^* for the complete range of admissible speeds for a dynamic shear crack. The expression for R/R_0^* for the sub-Rayleigh range was obtained from the study of *Rice et al.* [2005, equation 14]. R/R_0^* undergoes Lorentz-like contraction in the sub- Rayleigh regime, diminishing to zero at the Rayleigh wave speed c_R. The speed range between c_R and c_s, the S wave speed, is inadmissible on energetic grounds for a steady shear crack. Beyond c_s, R/R_0^* monotonically diminishes to zero again as the rupture speed approaches the P wave speed. For the supershear speed range inferred from various earthquakes, between 1.5 and $1.7c_s$, R/R_0^* lies between 0.3 and 0.6. Estimates of R_0^* by *Rice et al.* [2005], for the event set of *Heaton* [1990], vary between 1.3 and 36 m (with an uncertainty of factor of 2 since this value depended on R/L). This was obtained under the assumption of high peak strength and low residual strength implying $(\tau_p - \tau_r) \approx \tau_p = f_s\overline{\sigma}_n$ where $f_s = 0.6$ and $\sigma macr;_n$ is the effective normal pressure calculated at median depth for each of the earthquakes in the set. For low strength drop case, their estimates of R_0^* varied between 73 m and 3.3 km.

[36] We evaluate the spatial slip distribution $\Delta u(x)$ on the fault by numerically integrating the expression for slip velocity, $V = \partial\Delta u/\partial t = -v_r\partial\Delta u/\partial x$. This spatial distribution of slip is then used along with the spatially linear failure criterion used in our model to determine the slip-weakening law implied by our model. Figure 16 shows this slip-weakening behavior. There is little deviation from the linear slip-weakening law that is often (but somewhat arbitrarily) assumed in numerical simulations of dynamic shear ruptures, regardless of the choice of R/L. There is also some sensitivity to rupture velocity in the slip-weakening curves unlike the sub-Rayleigh case, but that too is modest.

8. Summary and Conclusions

[37] We have studied here the off-fault stressing induced by a two-dimensional steady slip pulse propagating at supershear speeds in a homogeneous isotropic elastic medium with a linear strength degradation boundary condition like in Figure 1. This work is an extension of the model of *Rice et al.* [2005] which looked at the sub-Rayleigh speed regime. Unlike its sub-Rayleigh analogue, the dependence on rupture velocity, as v_r/c_s, and the relative size of the slip-weakening zone, as R/L, for the elastic field of a supershear slip pulse are inseparable.

[38] Because of the supershear nature of the pulse, Mach fronts develop at the two ends of the slip pulse and, because our model is two-dimensional and at steady state, the elastic field within this band of Mach fronts does not attenuate with distance (practically up to distances comparable to the seismogenic zone depth) leading to a unique feature of the supershear slip pulse. We expect significant effects of the supershear slip pulse to be observed as damage at large distances. *Bernard and Baumont* [2005] also show, in their analytic and numerical model for kinematic ruptures, that the ground acceleration due to a supershear rupture is unusually high at distances of the order of few tens of

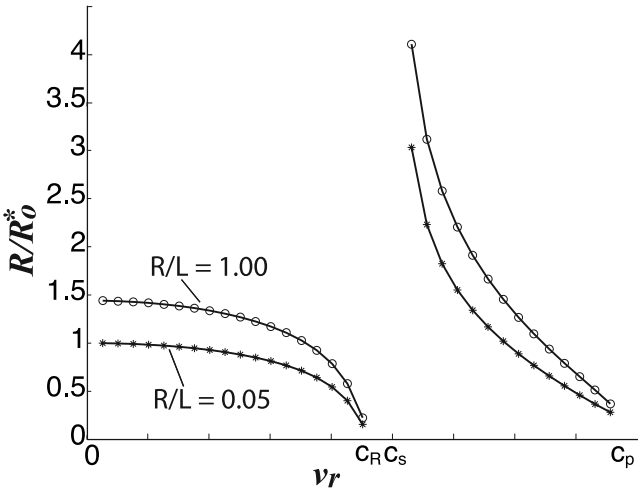

Figure 15. Variation in the scaled size of the process zone R/R_0^* with rupture velocity v_r. R_0^* is the size of the process zone at static limit for a semi-infinite shear crack. c_R, c_s, and c_p are the Rayleigh and S- and P-wave speeds of the medium, respectively.

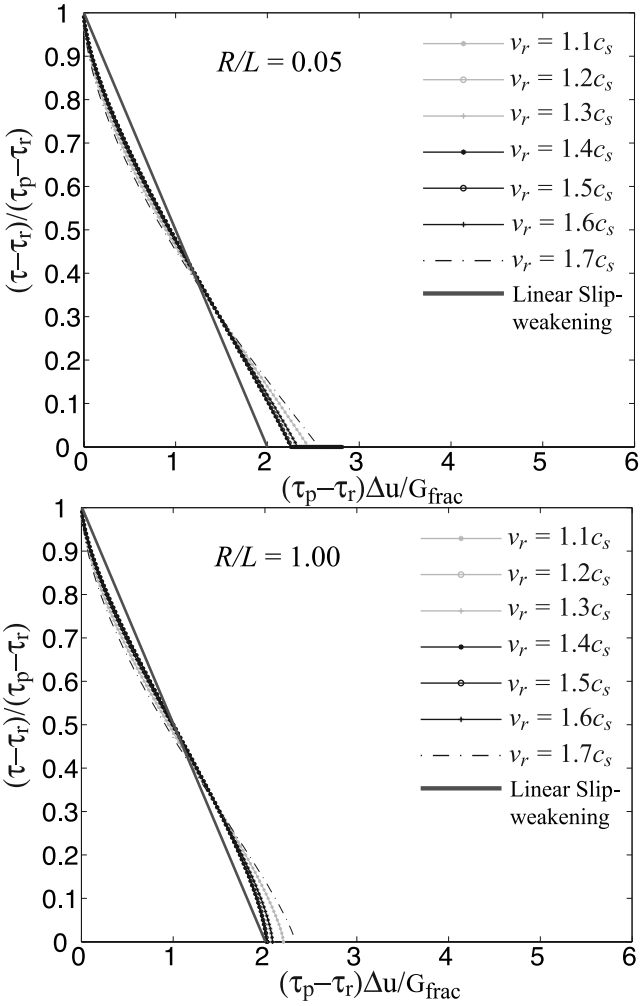

Figure 16. Slip-weakening law implied by our analysis compared with the linear slip-weakening law for $R/L = 0.05$ and 1.00.

kilometers. We observe that this feature is consistent with extension-like failure features observed a few kilometers away from the Kunlun fault during the 2001 Kokoxili event, thus lending support to the suggestion that its rupture speed was supershear in that region. We used our slip pulse model to also examine the simultaneous normal faulting observed during the 2001 Kokoxili event. However, that strand, lying parallel to the main strike-slip fault on the extensional side, does not experience positive change in Coulomb stress, so the specific features of supershear rupture do not provide an alternative to the slip partitioning explanation of that feature [*King et al.*, 2005].

[39] We also evaluated the change in Coulomb stress, in the medium hosting the slip pulse, on optimally oriented structures allowing for out-of-plane failure too. Failure is encouraged ($\Delta CS > 0$) mainly on the extensional side of the fault and increases in extent with increasing rupture velocity (v_r) and decreasing R/L. Increasing angle of orientation of the maximum in-plane principal compressive stress (Ψ) with the slip pulse results in the switching of the zone of $\Delta CS > 0$ from the compressional to the extensional side of the slip pulse.

[40] We also evaluated the radiated seismic energy and fracture energy due to a supershear slip pulse for a fixed dynamic stress drop (scaled by the strength drop), $(\sigma^0_{yx} - \tau_r)/(\tau_p - \tau_r) = 0.3$, and showed that the total of radiated and fracture energy decreases monotonically with increasing rupture velocity. Using those results, we also showed that the size of the slip-weakening zone decreases monotonically too with increasing rupture velocity in the supershear regime. We also showed that our spatially linear failure criterion deviates very little from the linear slip-weakening behavior regardless of the choice of R/L.

Appendix A: Determination of Coulomb Stress (CS) on a Given Plane

[41] Consider a fault plane Σ lying in a three-dimensional space (Figure A1). Let x, y, and z form a right-handed coordinate system where the surface of the Earth is in the x-y plane and the z axis points vertically upwards from the Earth's surface. The strike direction $\vec{s}$ is chosen along the surface trace of the fault plane such that the dip, defined below, is $\leq 90°$. Let $\vec{s}$ make an angle of ϕ with the x axis (measured positive for counterclockwise rotation about z), and let γ be the dip of the faulting plane, measured positive for right-handed rotation about the strike direction (i.e., angle from the Earth's surface at right of the strike direction to the fault plane). The positive strike direction is always chosen such that $0 < \gamma \leq 90°$. Let Σ^+ and Σ^- be the positive and the negative side of the fault plane, respectively (Figure A1a); Σ^- is the footwall (or is assigned arbitrarily if $\gamma = 90°$).

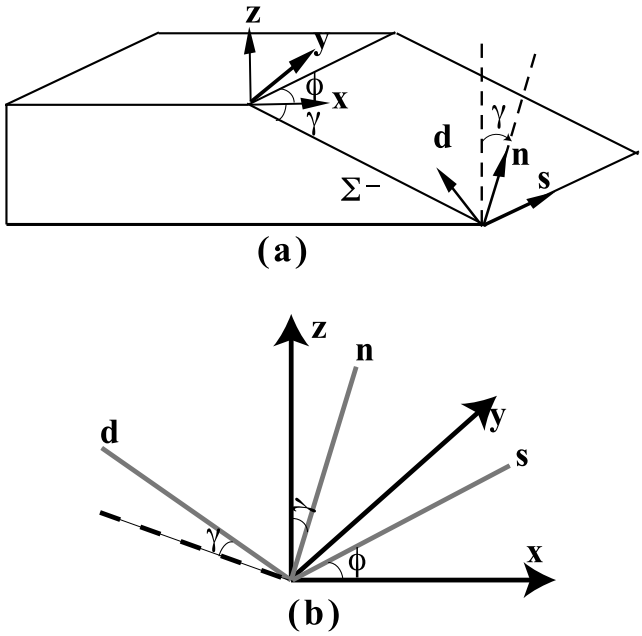

Figure A1. (a) Σ^- side of the fault plane, taken as the footwall for the dipping fault, and chosen arbitrarily if the fault is vertical. ϕ is the angle measured from the x axis to the surface trace of the fault corresponding with strike direction $\vec{s}$, counterclockwise about z. γ is the angle from the x-y plane, at the right of the strike direction, to the fault plane. s, d and n are the strike, updip, and outward normal vectors, respectively, to the Σ^- surface. (b) Various angles between the (s, d, n) and (x, y, z) coordinate systems.

[42] Let $\vec{n}$ be the unit normal to the fault plane directed from Σ^- to Σ^+. This will imply that any traction calculated with respect to this vector represents the action on the Σ^- plane due to the Σ^+ plane.

[43] Looking at Figure A1b, the z axis component of $\vec{n}$ is cos γ. The component of $\vec{n}$ on the x-y plane is then sin γ. Since this component is perpendicular to $\vec{s}$, the strike vector, the projections of $\vec{n}$ on the x and y axes are sinφsinγ and $-$cosφsinγ, respectively. Thus

$$\vec{n} = (\sin\phi\sin\gamma)\hat{i} + (-\cos\phi\sin\gamma)\hat{j} + (\cos\gamma)\hat{k} \tag{A1}$$

The unit vector acting along the strike direction is then given by (Figure A1b)

$$\vec{s} = (\cos\phi)\hat{i} + (\sin\phi)\hat{j} + (0)\hat{k} \tag{A2}$$

Then the vector acting along the updip direction is simply given by $\vec{d} = \vec{n} \times \vec{s}$ which is

$$\vec{d} = (-\sin\phi\cos\gamma)\hat{i} + (\cos\phi\cos\gamma)\hat{j} + (\sin\gamma)\hat{k} \tag{A3}$$

[44] The traction acting on the fault plane is then given by $T_i = \sigma_{ji}n_j$ where σ_{ij} are the components of the stress tensor (tensile positive) in the original x-y-z coordinate system. The normal stress on the fault plane is then given by $\sigma = T_i n_i$.

[45] The maximum shear stress acting on the plane is given by $\tau_{\max} = \sqrt{\tau_s^2 + \tau_d^2}$ where τ_s (= $T_i s_i$) and τ_d (= $T_i d_i$) are the shear stresses acting along the strike and the updip directions, respectively. Define rake angle (λ) as the angle between the unit slip vector $\vec{\xi}$ (slip vector $\delta\ \vec{u}$ is defined = $\vec{u}^+ - \vec{u}^-$ where $\vec{u}$ is the displacement vector) and $\vec{s}$ measured positive from the strike direction to that of $\vec{\xi}$ for counterclockwise rotation about the $\vec{n}$ direction.

[46] In terms of the rake angle (λ), the unit slip vector $\vec{\xi}$ is given by $\vec{\xi} = \vec{s}\cos\lambda + \vec{d}\sin\lambda$ and the shear stress in the slip direction is given by $\tau = T_i\xi_i$.

[47] It is then clear that a rake angle of 0 or π would result in pure left or right lateral faulting, respectively, and a rake angle of $-\pi/2$ or $\pi/2$ would result in pure normal or thrust faulting, respectively.

[48] The CS is now given by CS = $\tau + f_s\sigma$ where f_s is the static friction coefficient of the fault plane. τ is positive when slip occurs in the direction of the unit slip vector, and σ is positive when the fault is unclamped.

[49] The above methodology may be used in circumstances for which the fault plane is given and the geological sense of motion along it is known and is assumed to be active after stress change.

A1. CS on Optimal Mohr-Coulomb Planes

[50] From Mohr-Coulomb failure theory, it is known that for optimally oriented planes for failure (planes on which CS is maximum), the unit normals make angles of $\beta = \pm(\pi/4 + \varphi/2)$ (where tan $\varphi = f_s$) with the maximum compressive stress direction, and their line of intersection aligns with the intermediate principal stress direction. The slip vectors of the conjugate planes are in the plane comprising the maximum and minimum compressive stress directions (Figure A2).

[51] The shear and normal stresses on these planes are then given by

$$\begin{aligned}\tau &= \frac{(\sigma_1 - \sigma_3)}{2}\sin 2\beta \\ \sigma &= \frac{(\sigma_1 + \sigma_3)}{2} + \frac{(\sigma_1 - \sigma_3)}{2}\cos 2\beta\end{aligned} \tag{A4}$$

where $\sigma_1 \geq \sigma_2 \geq \sigma_3$ are the principal stresses and (like σ) are positive if tensile.

[52] Application to plane strain in the x-y plane aligned with the Earth's surface

[53] Case 1. $\sigma_1 = \sigma_{zz}$ (least compressive stress normal to the surface). This case results in pure thrust faulting, and both the conjugate planes are thrust faults. The strike of the two planes are along $\pm\vec{v}_2$ where $\vec{v}_2$ is the eigenvector corresponding to the intermediate principal stress σ_2. The dip is $\pi/2$.

[54] Case 2. $\sigma_2 = \sigma_{zz}$. This case results in strike-slip faulting, and the conjugate planes strike left laterally and right laterally. The strike of the two planes makes an angle of $\pm(\pi/2)$ with the maximum compressive stress (σ_3) direction. The dip is $\pi/2$.

[55] Case 3. $\sigma_3 = \sigma_{zz}$ (most compressive stress normal to the surface). This case results in pure normal faulting, and both the conjugate planes are normal faults. The strike of the two planes are given by $\pm\vec{v}_2$ where $\vec{v}_2$ is the eigenvector corresponding to the intermediate principal stress σ_2. The dip is $\pi/4 + \varphi/2$.

A2. Determination of the Change in Coulomb Stress (ΔCS) due to an Earthquake Rupture

[56] Case when fault plane and candidate direction of slip is known: Let $\boldsymbol{\sigma}_{ij}^0$ be the initial stress state (in the x-y-z system) and $\Delta\sigma_{ij}$ be the perturbation to the stress-field due to an earthquake rupture. Then ΔCS is given by ΔCS = $\Delta\tau + f_s\Delta\sigma$ where $\Delta\tau$ and $\Delta\sigma$ are given by $\Delta\tau = \Delta\sigma_{ij}n_i\xi_j$ and $\Delta\sigma = \Delta\sigma_{ij}n_i n_j$. The vectors $\vec{n}$ and $\vec{\xi}$ are defined in the first section.

[57] Case when fault planes are optimally oriented: We first begin by determining the conjugate failure planes for the total stress state, i.e., for $\sigma_{i\,j} = \sigma_{ij}^0 + \Delta\sigma_{ij}$. Let $\vec{v}_1$ and $\vec{v}_3$ be the eigenvectors associated with the minimum and maximum principal stresses, respectively, of the total stress state. The failure plane normals are then obtained by rotating $\vec{v}_3$ about $\vec{v}_2$ by an angle of $\pm(\pi/4^\circ + {}^\circ\varphi/2)$. Let $\vec{n}_1$ and $\vec{n}_2$ be the outward unit normals to the conjugate planes and $\vec{\xi}_1$ and $\vec{\xi}_2$ be the unit vectors in the direction of slip on the $\sigma_{1/2}^+$ planes, respectively (Figure A2). Then

$$\vec{\xi}_1 = \vec{\nu}_3\cos(\pi/4 - \varphi/2) + \vec{\nu}_1\sin(\pi/4 - \varphi/2) \tag{A5}$$

$$\vec{n}_1 = -\vec{\nu}_3\cos\,(\pi/4 + \varphi/2) + \vec{\nu}_1\sin(\pi/4 + \varphi/2) \tag{A6}$$

$$\vec{\xi}_2 = \vec{\nu}_3\cos(\pi/4 - \varphi/2) - \vec{\nu}_1\sin(\pi/4 - \varphi/2) \tag{A7}$$

$$\vec{n}_2 = -\vec{\nu}_3\cos(\pi/4 + \varphi/2) - \vec{\nu}_1\sin(\pi/4 + \varphi/2) \tag{A8}$$

ΔCS is then calculated for each of the optimal planes by ΔCS = $\Delta\tau + f_s\Delta\sigma$ where $\Delta\tau$ and $\Delta\sigma$ are given by $\Delta\tau = \Delta\sigma_{ij}n_i\xi_j$ and $\Delta\sigma = \Delta\sigma_{ij}n_i n_j$. n_i, ξ_i are the components of the unit nor-

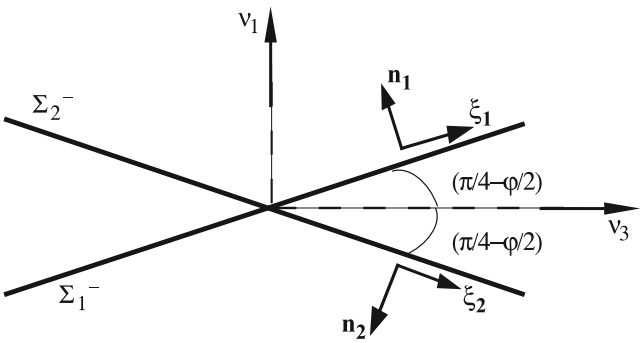

Figure A2. Optimally oriented conjugate planes (Σ_1 and Σ_2) for failure. $\vec{\nu}_1$ and $\vec{\nu}_3$ are the eigenvectors corresponding to the minimum and maximum principal compressive stresses, respectively. $\vec{n}_1, \vec{\xi}_1$, and $\vec{n}_2, \vec{\xi}_2$ are the unit normal and unit slip vectors, respectively, to the conjugate planes. $\tan\varphi = f_s$ where f_s is the coefficient of friction for the planes.

mal and unit slip vectors, respectively, for each of the optimal planes. The maximum of the two ΔCS values is then sometimes identified as the plane more likely to slip because of an earthquake rupture, although we see no firm basis for that. However, this is not the only way the change in Coulomb stress on optimal planes can be identified. The different conjugate fault plane orientations can be determined for stress states both before (σ^0_{ij}) and after the rupture (σ_{ij}), and then the Coulomb stress changes can be evaluated as $\Delta\mathrm{CS} = (\mathrm{CS})^{\sigma 0 + \Delta\sigma}_{\mathrm{optimal}} - (\mathrm{CS})\sigma^0_{\mathrm{optimal}}$. This would give a unique value of ΔCS regardless of the optimal plane chosen in each of the stress states. Our contour plots here use the first method.

Appendix B: Far-Field (Nonattenuating Part of) Stresses in Band Between Mach Fronts

[58] In their study of a supershear slip pulse, propagating at steady state in a two-dimensional homogeneous isotropic medium under plane strain conditions, *Dunham and Archuleta* [2005] have shown that the off-fault velocity fields trace out the exact slip velocity during the passsage of the *S* wavefront. This means that a nonattenuating field, caused by the passage of the *S* wavefront, is traced out in the medium, through which the slip pulse passes, and extends, theoretically, to infinity. Nevertheless, this observation points out that significant effects of the supershear slip pulse can be observed at large distances away from it unlike its sub-Rayleigh analogue where both the *P* wave and the *S* wave stress fields attenuate as $1/r$ with distance from the source r. In the following section, we re-express the far-field stress distribution in terms of the slip velocity distribution on the fault. Let $V(x)$ be the slip rate along the rupture and Δu the slip, i.e.,

$$\begin{aligned} V(x) &= (\partial u_x/\partial t)^+ - (\partial u_x/\partial t)^- \\ &= -v_r\left[(\partial u_x/\partial x)^+ - (\partial u_x/\partial x)^-\right] \\ &= -2v_r(\partial u_x/\partial x)^+ = -2v_r\epsilon^{\mathrm{fault}}_{xx} \\ &= -2v_r\left[\frac{1-\nu}{2\mu}\sigma^{\mathrm{fault}}_{xx}\right] \\ &= -\left[v_r\left(\hat{\alpha}_s^2+1\right)/(2\mu\alpha_d)\right]\Im S(z_s) \end{aligned} \tag{B1}$$

using $v^\circ = {}^\circ 0.25$ and equation (1). $S(z_s)$ is given by equation (2) in section 2, and $z_s = x + i0^+$, the limit as we approach the fault from $y > 0$, in order to get the sign of $\Im S(z_s)$ correct. Solving for $\Im S(z_s)$ and using this in equation (1) (ignoring the *P* wave contribution) with $z_s = x + \alpha_s|y|$, the far-field stress changes are

$$\begin{aligned} \Delta\sigma^{\mathrm{far}}_{xx} &= -\mu(v_r^2 - 2c_s^2)V(z_s)\mathrm{sign}(y)/v_r^3 \\ \Delta\sigma^{\mathrm{far}}_{yx} &= -\mu(v_r^2 - 2c_s^2)^2 V(z_s)/(2v_r^3 c_s^2\hat{\alpha}_s) \\ \Delta\sigma^{\mathrm{far}}_{yy} &= -\Delta\sigma_{xx} \\ \Delta\sigma^{\mathrm{far}}_{zz} &= 0 \end{aligned} \tag{B2}$$

[59] Because $V(x)$ is always positive in our cases, $\Delta\sigma^{\mathrm{far}}_{xx}$ and $\Delta\sigma^{\mathrm{far}}_{yy}$ change signs as v_r increases past $\sqrt{2}c_s$, but $\Delta\sigma^{\mathrm{far}}_{yx}$ is negative for all v_r, except for $\sqrt{2}c_s$ at which all the $\Delta\sigma^{\mathrm{far}}_{kl}$ vanish. The expressions predict that when $v_r > \sqrt{2}c_s$, the sign of the far-field $\Delta\sigma^{\mathrm{far}}_{xx}$ is the same as that along the rupture surface on the corresponding side of the fault, but that the sign is reversed when $v_r < \sqrt{2}c_s$. It can also be quite easily shown that the far-field stress perturbation $\Delta\sigma^{\mathrm{far}}_{xx} =$

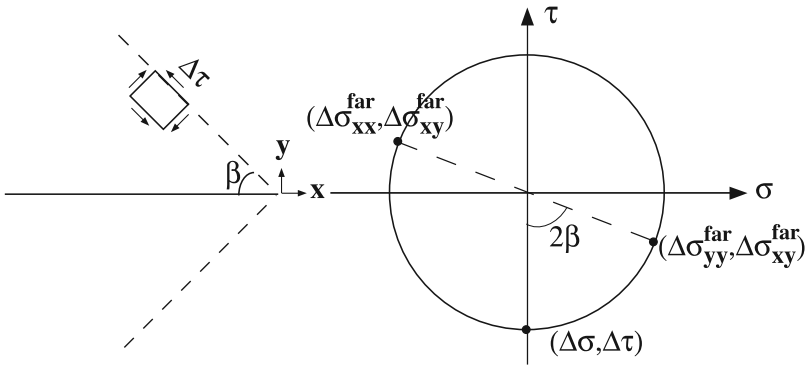

Figure B1. Stresses acting on an element aligned with the Mach fronts and in the Cartesian system. $\Delta\tau$ is the shear stress acting on the element in that orientation and $\Delta\sigma$ is the normal stress (=0). β is the inclination of the Mach front with respect to the slip pulse. $\Delta\sigma^{\mathrm{far}}_{xy}$ and $\Delta\sigma^{\mathrm{far}}_{yy}$ are the shear and normal stress in the far field measured with respect to the x-y coordinates. For the Mohr's circle, we use tensile positive convention. Note that $\Delta\tau > 0$ when $v_r < \sqrt{2}c_s$ and changes sign at higher speeds crossing zero at $v_r = \sqrt{2}c_s$.

$0.75(1-2\sin^2\beta)\Delta\sigma_{xx}^{\text{on-fault}}$, where β is the Mach angle, $\sin\beta = c_s/v_r$. Thus at velocities close to $\sqrt{2}c_s$, the far-field stress perturbation is still a significant percentage of the same on the fault.

[60] We note that an alternative way to derive the ratio of far-field shear to normal stresses is to employ Mohr's circle concepts. We know that for an element of material, in the medium in which a steady state supershear rupture is propagating, one of whose faces is aligned with the Mach front (in $y > 0$ say), the stress component that jumps in value as the Mach front is crossed is the shear stress acting on it. The shear and normal stresses in the Cartesian coordinate system for this element is then obtained by rotating it about the center by an angle β. This translates to a rotation in the Mohr's circle plane by an angle of 2β. Thus if $\Delta\tau$ is the shear stress acting on the element aligned with the Mach front, then $\Delta\sigma_{yy}^{\text{far}} = \Delta\tau\sin(2\beta)$ and $\Delta\sigma_{yx}^{\text{far}} = -\Delta\tau\cos(2\beta)$. Thus $\Delta\sigma_{yx}^{\text{far}}/\Delta\sigma_{yy}^{\text{far}} = -\cot(2\beta)$ (Figure B1). Using the results above, we can now make some estimates on far-field stress perturbations left in the wake of a supershear slip pulse. Some assumptions need to be made before making estimates of the far-field stress values. First, we shall use the maximum slip velocities obtained from our model for small ($R/L = 0.05$) and large ($R/L = 1.0$) values of the process zone (R) with respect to the length of the slip pulse (L) (Figure 6). Slip velocity V in our model is nondimensionalized as $\mu V/[(\sigma_{yx}^0 - \tau_r)c_s]$, where μ is the shear modulus of the medium, $(\sigma_{yx}^0 - \tau_r)$ is the dynamic stress drop, and c_s is the shear wave speed of the medium. We assume that $\mu = 30$ GPa, $(\sigma_{yx}^0 - \tau_r) = 3$ MPa, and $c_s = 3$ km/s. This gives us maximum slip velocity values varying from 0.5 to 10.5 m/s and increasing with increasing rupture velocity.

[61] Using the above values of slip velocity, one can now make reasonable estimates of far-field stresses (Figure 6). This provides some interesting results. First, the perturbation in the shear stress field $\Delta\sigma_{xy}^{\text{far}}$ is always negative in the far field as expected earlier. $\Delta\sigma_{xx}^{\text{far}}$ changes sign from being extensional ($\Delta\sigma_{xx}^{\text{far}} > 0$) to compressional as one crosses the $\sqrt{2}c_s$ rupture velocity value. The magnitude of the stress perturbation is also quite high, varying between -17 and 8 MPa (using the maximum value of slip velocity). Also, the changes in the far-field stresses seem to be very sensitive to the rupture velocity. For example, $\Delta\sigma_{xx}^{\text{far}}$ increases from 1 to 3 MPa as the rupture velocity changes from $1.45c_s$ to $1.5c_s$. Of course, the slip velocity also changes here as the rupture velocity changes. Hence it is useful to know the change in the stress field for fixed value of peak slip velocity and slightly different values of rupture velocity. Taking $V = 5$ m/s as representative of the faster slip velocities, we get the rough estimates for $v_r = 1.51c_s$ to $1.61c_s$ (on the compressional side of the fault),

$$\begin{aligned}\Delta\sigma_{xx}^{\text{far}} &= -(4.0 \text{ to } 7.0 \text{ MPa})\text{sign}(y)\\ \Delta\sigma_{yx}^{\text{far}} &= -(0.4 \text{ to } 1.5 \text{ MPa})\\ \Delta\sigma_{yy}^{\text{far}} &= +(4.0 \text{ to } 7.0 \text{ MPa})\text{sign}(y)\end{aligned} \tag{B3}$$

[62] Those are large normal stress changes, 40 bars at $1.51c_s$, and 70 bars at $1.61c_s$, especially given that they do not attenuate with distance until three-dimensional effects enter the model. For $v_r = 1.21$ to $1.31c_s$, the normal stress changes have the same magnitude range but reverse sign from those above. The estimates are peak stress values; average stress changes, if V_{average} is about 1 m/s, would be a fifth as large, but still significant at about 10 bars.

[63] **Acknowledgments.** The study at Harvard was supported by NSF-EAR grant 0440145. We thank Eric Dunham for comments on supershear solution, Nathan Benesh for a clarifying discussion of different ways of calculating Coulomb stress changes for optimally oriented structures, and Michel Bouchon for discussion of his seismic inversion with M. Vallée for the 2001 Kokoxili event. We are also grateful for review comments from Steve Day, David Oglesby, and an anonymous reviewer.

References

Andrews, D. J. (1976), Rupture velocity of plane strain shear cracks, *J. Geophys. Res.*, *81*, 5679–5687.

Andrews, D. J. (1985), Dynamic plane-strain shear rupture with a slip-weakening friction law calculated by a boundary integral method, *Bull. Seismol. Soc. Am.*, *75*, 1–21.

Antolik, M., R. E. Abercrombie, and E. Ekstrom (2004), The 14 November 2001 Kokoxili (Kunlunshan), Tibet, earthquake: Rupture transfer through a large extensional step-over, *Bull. Seismol. Soc. Am.*, *94*(4), 1173–1194.

Archuleta, R. J. (1984), A faulting model for the 1979 Imperial Valley earthquake, *J. Geophys. Res.*, *89*, 4559–4585.

Bhat, H. S., R. Dmowska, J. R. Rice, and N. Kame (2004), Dynamic slip transfer from the Denali to Totschunda Faults, Alaska: Testing theory for fault branching, *Bull. Seismol. Soc. Am.*, *94*(6B), S202–S213.

Bernard, P., and D. Baumont (2005), Shear Mach wave characterization for kinematic fault rupture models with constant supershear rupture velocity, *Geophys. J. Int.*, *162*, 431–447.

Bouchon, M., and M. Vallee (2003), Observation of long supershear rupture during the magnitude 8.1 Kunlunshan earthquake, *Science*, *301*(5634), 824–826.

Bouchon, M., N. Toksoz, H. Karabulut, M. P. Bouin, M. Dietrich, M. Aktar, and M. Edie (2000), Seismic imaging of the 1999 Izmit (Turkey) rupture inferred from the near-fault recordings, *Geophys. Res. Lett.*, *27*, 3013–3016.

Bouchon, M., M. P. Bouin, H. Karabulut, M. N. Toksoz, M. Dietrich, and A. Rosakis (2001), How fast is rupture during an earthquake? New insights from the 1999 Turkey earthquakes, *Geophys. Res. Lett.*, *28*, 2723–2726.

Broberg, K. B. (1978), On transient sliding motion, *Geophys. J. R. Astron. Soc.*, *52*, 397–432.

Broberg, K. B. (1989), The near-tip field at high crack velocities, *Int. J. Fract.*, *39*, 1–13.

Broberg, K. B. (1999), *Cracks and Fracture*, Elsevier, New York.

Burridge, R. (1973), Admissible speeds for plane-strain shear cracks with friction but lacking cohesion, *Geophys. J. R. Astron. Soc.*, *35*, 439–455.

Burridge, R., G. Conn, and L. B. Freund (1979), The stability of a rapid mode II shear crack with finite cohesive traction, *J. Geophys. Res.*, *85*, 2210.

Dunham, E. M., and R. J. Archuleta (2005), Near-source ground motion from steady state dynamic rupture pulses, *Geophys. Res. Lett.*, *32*, L03302, doi:10.1029/2004GL021793.

Ellsworth, W. L., M. Celebi, J. R. Evans, E. G. Jensen, D. J. Nyman, and P. Spudich (2004), Processing and modeling of the pump station 10 record from the November 3, 2002, Denali fault, Alaska earthquake, in Proceedings, 11th Intern. Conf. Soil Dynam. Earthq. Eng. 1, Berkeley, California, 471–477.

Eshelby, J. D. (1949), Uniformly moving dislocations, *Proc. Phys. Soc. A*, *62*, 307–314.

Freund, L. B. (1979), The mechanics of dynamic shear crack propagation, *J. Geophys. Res.*, *84*, 2199–2209.

Freund, L. B. (1990), *Dynamic Fracture Mechanics*, Cambridge Univ. Press, New York.

Heaton, T. H. (1990), Evidence for and implications of self-healing pulses of slip in earthquake rupture, *Phys. Earth Planet. Inter.*, *64*, 1–20.

Ida, Y. (1972), Cohesive force across the tip of a longitudinal-shear crack and Griffith's specific surface energy, *J. Geophys. Res.*, *77*, 3796–3805.

Kame, N., J. R. Rice, and R. Dmowska (2003), Effects of pre-stress state and rupture velocity on dynamic fault branching, *J. Geophys. Res.*, *108*(B5), 2265, doi:10.1029/2002JB002189.

Kikuchi, M., and Y. Yamanaka (2001), Special Event Page, 2001/11/14 Qinghai Xinjiang Border, China, wwweic.eri.u-tokyo.ac.jp/topics/200111140926, Earthquake Information Center, ERI, Univ. Tokyo, Japan.

King, G., Y. Klinger, D. Bowman, and P. Tapponnier (2005), Slip partitioned surface breaks for the 2001 Kokoxili earthquake, China (Mw 7.8), *Bull. Seismol. Soc. Am.*, *95*(2), 731–738.

Klinger, Y., X. Xu, P. Tapponnier, J. Van der Woerd, J. Lasserre, and G. King (2005), High-resolution satellite imagery mapping of the surface rupture and slip distribution of the M_w 7.8, November 14, 2001 Kokoxili earthquake (Kunlun Fault, Northern Tibet, China), *Bull. Seismol. Soc. Am.*, *95*(5).

Klinger, Y., R. Michel, and G. C. P. King (2006), Evidence for an earthquake barrier model from Mw ~7.8 Kokoxili (Tibet) earthquake slip-distribution, *Earth Planet. Sci. Lett.*, *242*, 354–364.

Lasserre, C., G. Peltzer, F. Cramp, Y. Klinger, J. Van der Woerd, and P. Tapponnier (2005), Co-seismic deformation of the Mw = 7.8 Kokoxili earthquake in Tibet, measured by SAR interferometry, *J. Geophys. Res.*, *110*(B12), B12408, doi:10.1029/2004JB003500.

Lin, A., B. Fu, J. Guo, Q. Zeng, G. Dang, W. He, and Y. Zhao (2002), Co-seismic strike-slip and rupture length produced by the 2001 M_s 8.1 Central Kunlun earthquake, *Science*, *296*(5575), 2015–2016.

Lin, A., M. Kikuchi, and B. Fu (2003), Rupture segmentation and process of the 2001 M_w 7.8 Central Kunlun, China, earthquake, *Bull. Seismol. Soc. Am.*, *93*(6), 2477–2492.

Muskhelishvili, N. I. (1953), Singular integral equations: boundary problems of function theory and their application to mathematical physics, Translation from the Russian edited by J. R. M. Radok, P. Noordhoff, Groningen.

Palmer, A. C., and J. R. Rice (1973), The growth of slip surfaces in the progressive failure of over-consolidated clay, *Proc. R. Soc. London, Ser. A*, *332*, 527–548.

Poliakov, A. N. B., R. Dmowska, and J. R. Rice (2002), Dynamic shear rupture interactions with fault bends and off-axis secondary faulting, *J. Geophys. Res.*, *107*(B11), 2295, doi:10.1029/2001JB000572.

Ratchkovski, N. A. (2003), Change in stress directions along the central Denali fault, Alaska after the 2002 earthquake sequence, *Geophys. Res. Lett.*, *30*(19), 2017, doi:10.1029/2003GL017905.

Rice, J. R. (1980). The Mechanics of Earthquake Rupture, Physics of the Earth's Interior (Proc. International School of Physics 'Enrico Fermi', Course 78, 1979; ed. A. M. Dziewonski and E. Boschi), Italian Physical Society and North-Holland Publ. Co., pp. 555–649.

Rice, J. R., C. G. Sammis, and R. Parsons (2005), Off-fault secondary failure induced by a dynamic slip-pulse, *Bull. Seismol. Soc. Am.*, *95*(1), 109134, doi:10.1785/0120030166.

Robinson, D. P., C. Brough, and S. Das (2006), The Mw 7.8, 2001 Kunlunshan earthquake: Extreme rupture speed variability and effect of fault geometry, *J. Geophys. Res.*, *111*, B08303, doi:10.1029/2005JB004137.

Rosakis, A. J., O. Samudrala, and D. Coker (1999), Cracks faster than the shear wave speed, *Science*, *284*, 1337–1340.

Tocheport, A., L. Rivera, and J. Van der Woerd (2006), A study of the 14 November 2001 Kokoxili earthquake: History and geometry of the rupture from teleseismic data and field observations, *Bull. Seismol. Soc. Am.*, *96*, 1729–1741.

Xu, X., W. Chen, W. Ma, G. Yu, and G. Chen (2002), Surface rupture of the Kunlunshan earthquake (Ms 8.1), northern Tibetan Plateau, China, *Seismol. Res. Lett.*, *73*, 884–892.

H. S. Bhat, R. Dmowska, and J. R. Rice, Division of Engineering and Applied Sciences, Harvard University, 327 Pierce Hall, 29 Oxford Street, Cambridge, MA 02138, USA. (bhat@esag.harvard.edu; dmowska@esag.harvard.edu; rice@esag.harvard.edu)

G. C. P. King and Y. Klinger, Laboratoire Tectonique, Institut de Physique du Globe de Paris, 4 place Jussieu, 75005, Paris, France. (king@ipgp.jussieu.fr; klinger@ipgp.jussieu.fr)